Cell migration dynamics explained by the coupling of mechanics with electrochemistry and pH regulation

Yizeng Li [1,*] and Sean X. Sun [2,3,4,†]

[1] *Department of Biomedical Engineering, Binghamton University, SUNY, Binghamton, New York 13902, USA*
[2] *Department of Mechanical Engineering, Johns Hopkins University, Baltimore, Maryland 21218, USA*
[3] *Institute for NanoBioTechnology, Johns Hopkins University, Baltimore, Maryland 21218, USA*
[4] *Center for Cell Dynamics, Johns Hopkins School of Medicine, Baltimore, Maryland 21205, USA*

(Received 31 July 2023; accepted 19 April 2024; published 13 May 2024)

Anisotropic environmental signals or polarized membrane ion/solute carriers can generate spatially varying intracellular gradients, leading to polarized cell dynamics. For example, the directional migration of neutrophils, galvanotaxis of glioblastoma, and water flux in kidney cells all result from the polarized distribution of membrane ion carriers and other intracellular components. The underlying physical mechanisms behind how polarized ion carriers interact with environmental signals are not well studied. Here, we use a physiology-relevant, physics-based mathematical model to reveal how ion carriers generate intracellular ion and voltage gradients. The model can discern the contribution of individual ion carriers to the intracellular pH gradient, electric potential, and water flux. We discover that an extracellular pH gradient leads to an intracellular pH gradient via chloride-bicarbonate exchangers, whereas an extracellular electric field leads to an intracellular electric potential gradient via passive potassium channels. In addition, mechanical-biochemical coupling can modulate actin distribution and flow, creating a biphasic dependence of cell speed on water flux. Moreover, we find that F-actin interaction with NHE alone can generate cell movement, even when other ion carriers are not polarized. Taken together, the model highlights the importance of cell ion dynamics in modulating cell migration and cytoskeletal dynamics.

DOI: 10.1103/PhysRevResearch.6.023158

I. INTRODUCTION

In cells, the spatial distributions of proteins and organelles are often not uniform. A polarized cell is essential in many (patho)physiological processes such as morphogenesis, immune response, nutrient delivery and filtration, signal transduction, and cancer metastasis [1,2]. Many studies have examined how extracellular biochemical signals generate cell polarization and establish intracellular gradients [3]. Cell polarity influences cell cytoskeletal structure, force distribution, morphology, and migration [4–9]. Recent works have shown that even in the absence of extracellular signals, the extracellular fluid influences cell polarity, giving a polarized distribution of ion channels, exchangers, and pumps [10–13]. (Here, we will refer to these ion channels, exchangers, and pumps as membrane ion carriers.) Epithelial cells and cells in confinement display polarized distributions of ion carriers at the two ends of the cells without extracellular signal gradients [11,14–16]. In contrast, unconfined cells on two-dimensional substrates show a lesser degree of ion carrier polarization [17]. Polarized ion carriers can generate water fluxes across the cell membrane, contributing to processes such as cell shape change, epithelial fluid transport, and water-driven cell migration.

Since fluxes through ion carriers (and thus water) are affected by electric potential, any external electric fields will also generate intracellular ion gradients. Moreover, fluxes of major ions such as sodium, potassium, and chloride are influenced by proton flux. Since the tumor microenvironment often has an elevated pH [18], and leukocytes [19,20] and cancer cells [14–17] both utilize sodium-hydrogen exchangers to migrate, it is important to understand how environmental pH changes influence cell ion homeostasis and migration. In this paper, we determine how extracellular electric potential and pH gradients affect intracellular ion distribution through ion carriers using a theoretical model [Fig. 1(a)]. We also quantify how a polarized distribution of ion carriers can generate intracellular gradients without external signals [Fig. 1(a)]. Since ions often interact strongly with proteins and genetic material, intracellular ion gradients will contribute to intracellular protein biochemical gradients.

In addition to confinement, polarized ion carriers can occur through spatially varying F-actin assembly and disassembly, which not only regulate the distribution of ion carriers through vesicular trafficking but also through direct physical interaction with membrane-embedded proteins [21]. Our earlier work demonstrated that actin colocalizes with sodium-hydrogen exchangers in confined breast cancer cells [16] and with sodium-potassium pumps in kidney cells [11].

*yli33@binghamton.edu
†ssun@jhu.edu

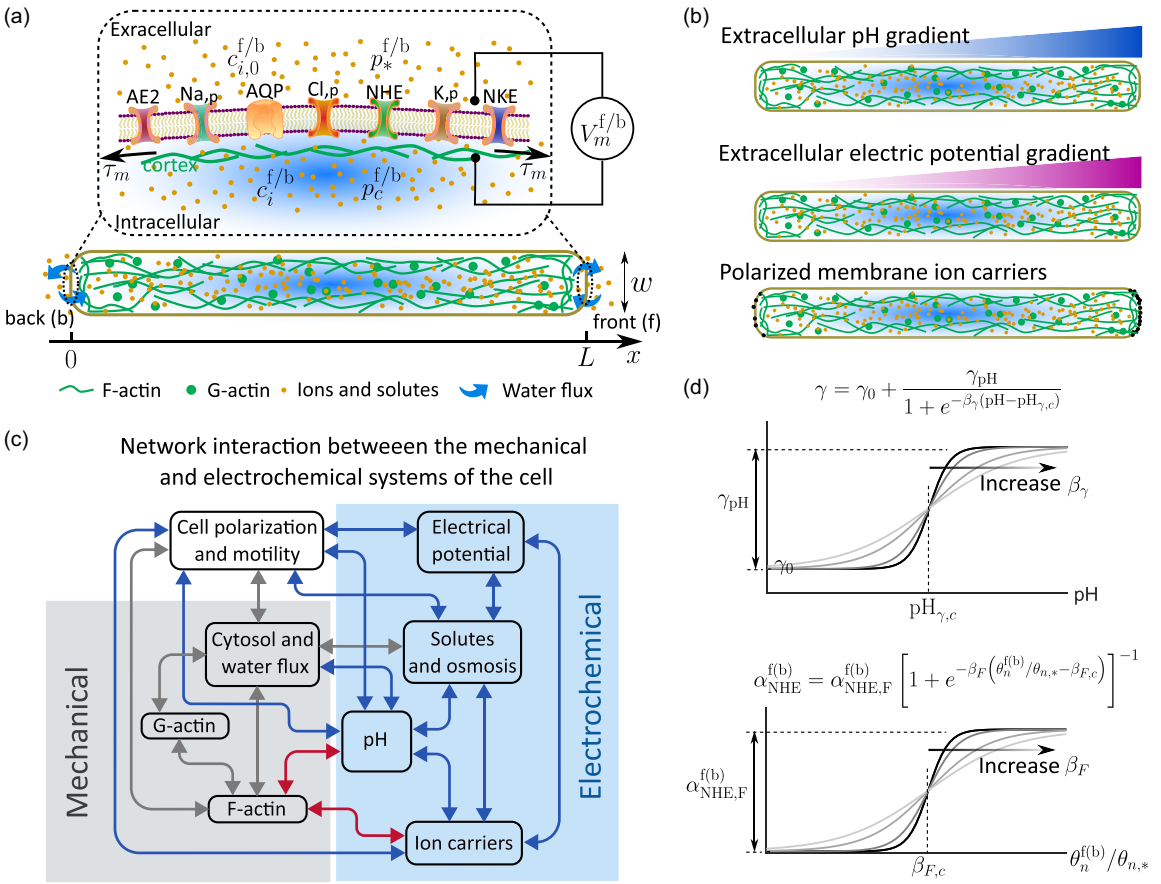

FIG. 1. (a) Schematics of a confined cell of length L and width w (not to scale). $\mathrm{Na,p}$: passive sodium channel. $\mathrm{K,p}$: passive potassium channel. $\mathrm{Cl,p}$: passive chloride channel. NKE: sodium-potassium pump. NHE: sodium-hydrogen exchanger. AE2: chloride-bicarbonate exchanger. AQP: aquaporin. $V_m^{\mathrm{f/b}} = \phi^{\mathrm{f/b}} - \phi_0^{\mathrm{f/b}}$ is the membrane potential. c_i is the intracellular ion concentration for each ion species i. $c_{i,0}$ is the extracellular one evaluated at the cell membrane. p_c and p_* are, respectively, the hydrostatic pressure inside and outside of the cell at the cell boundaries. τ_m is the membrane tension, mostly contributed by the cortex. The cell front and back are defined at $x = L$ and $x = 0$, respectively. Actin polarization happens at the cell front only. (b) The scenarios studied in this work. Cells are exposed to extracellular pH or electric potential gradients, and/or exhibiting polarized membrane ion carriers. (c) Diagram of the model showing the network interaction between the mechanical and electrochemical systems of the cell. The gray lines are the coupling established in our prior works. The red lines indicate the new coupling represented by Eqs. (42) and (43). The blue lines show the new studies carried out in this work. (d) Features of the coupling functions in Eqs. (42) and (43). The diagrams show how each parameter affects the behaviors of the functions.

Polarization of ion carriers will, in turn, affect intracellular cell homeostasis and biochemical gradients, forming feedback loops.

A physiology-relevant, physics-based mathematical model has the potential to reveal cell migration mechanisms and provide unique insights into critical biophysical processes that are difficult to obtain from experiments. In this work, we use such a mathematical model to study the effects of (1) polarized ion carriers on cell migration and homeostasis, (2) polarized extracellular chemical-physical environment on cell polarization, and (3) actin-chemical coupling in cell polarization and water flux. The model predicts cell migration speed and cytoplasmic distributions of ion concentrations, pH, and electric potential. We will also answer an interesting question: can there be just one single ion carrier responsible for sensing the cell microenvironment? The model predictions will have medical or therapeutic implications where cell dynamics are regulated by pH or electric potential [22,23].

II. METHOD

A. Model overview

Here, we describe a steady-state cell migration model considering cytosol, F-actin, G-actin, charged ions, pH, and voltage. The model is applicable to confined cell migration, either in a narrow channel or three-dimensional extracellular matrix, where cells are elongated and migrate along one direction denoted as the x direction. All field variables are functions of x. We neglect changes in variables along directions perpendicular to cell migration. In many cases, space exists between the nucleus and the cell lateral wall, so the nucleus does not significantly block material transportation from one end of the cell to the other [14–16,24]. For this reason, we do not explicitly model the nucleus. The effect of the nucleus can be incorporated into the effective diffusion coefficients of ions and proteins, if desirable. It is also possible that the nucleus separates a cell's front and back compartments and develops

pressure differences within the cell [25,26]. Our model does not include this scenario.

The cell front is defined by where actin polymerization happens (at $x = L$), which is also the direction of cell migration without a strong water flow perturbation. We use superscripts "f" and "b" throughout the paper to represent quantities associated with the front and back ends of the cell, respectively. Under steady state, the cell velocity, $v_{\text{cell}} = \dot{x}^{\text{f}}(t) = \dot{x}^{\text{b}}(t)$, and the cell length, $x^{\text{f}}(t) - x^{\text{b}}(t) = L$, are constants. In our results, we use $x \in [0, L]$ to represent the cytoplasmic domain in the moving frame of the cell [Fig. 1(b)]. Quantities associated with the extracellular environment will be denoted by a subscript "0." In this work, we consider a more involved model compared to our early works [15–17,27–29]. This model emphasizes the coupling among the mechanical, electrical, and chemical properties of a cell and how the polarization of one aspect of the cell affects the other properties and cell migration. The model neglects the impact of a cell on the extracellular biochemical environment. This is based on the assumption that the extracellular concentrations balance on a longer spatial scale than the intracellular ones. To ensure comprehensive coverage, we present the complete model in this "Method" section, with a focus on highlighting new elements introduced in this study. Readers primarily interested in gaining modeling insights into biological processes are encouraged to proceed directly to the "Results and Discussion" section.

The primary variables, or unknowns to be solved, of the model are

$$\mathbf{X} = \{p_c(x),\, v_c,\, v_n(x),\, \theta_n(x),\, \theta_c(x),\, c_{\text{Na}}(x),\, c_{\text{K}}(x),\, c_{\text{Cl}}(x),\, \text{pH}(x),\, c_A(x),\, c_{\text{Buf}}(x),\, \phi(x),\, v_{\text{cell}}\}^{\text{T}}, \tag{1}$$

where $p_c(x)$ is the hydrostatic pressure (Pa) of the cytosol, v_c is the velocity (nm/s) of the cytosol, $v_n(x)$ is the velocity (nm/s) of F-actin, $\theta_n(x)$ is the concentration (mM) of actin in the filamentous form (F-actin), $\theta_c(x)$ is the concentration (mM) of actin in the monomeric form (G-actin), $c_{\text{Na}}(x)$ is the concentration (mM) of Na^+ in the cytosol, $c_{\text{K}}(x)$ is the concentration (mM) of K^+ in the cytosol, $c_{\text{Cl}}(x)$ is the concentration (mM) of Cl^- in the cytosol, $\text{pH}(x)$ is the intracellular pH, $c_A(x)$ is the concentration (mM) of nonpermeable proteins, A^-, in the cytosol, $c_{\text{Buf}}(x)$ is the concentration (mM) of deprotonated buffer ions, Buf^-, in the cytosol, $\phi(x)$ is the intracellular electric potential (mV), and v_{cell} is the steady-state cell migration velocity (nm/s).

These variables will be solved through a set of coupled nonlinear equations, which we will describe in detail below. All other variables can be derived from these primary variables. This model does not include myosin dynamics but can be expanded to include it if necessary, as we have developed in our prior work [30].

B. Cytosol mechanics

The cytosol is a waterlike fluid that exchanges with the extracellular water through membrane water flux. The relative motion between the cytosol and the actin network generates an interface stress proportional to the velocity difference of the two phases, i.e., $\eta\theta_n(v_c - v_n)$, where η is the coefficient of interfacial friction between the actin-network phase and the cytosol phase. When the interface stress is significantly larger than the cytosol viscous shear stress, the viscous shear stress can be neglected from the model. In this case, the pressure gradient of the cytosol balances the interfacial stress. The force and mass balances of the cytosol are

$$-\frac{dp}{dx} - \eta\theta_n(v_c - v_n) = 0, \quad \frac{dv_c}{dx} = 0. \tag{2}$$

The mass balance in the one-dimensional space, $dv_c/dx = 0$, suggests that $v_c(x) = v_c = \text{const}$. The flux boundary conditions for cytosol are

$$\begin{aligned} v_c - v_{\text{cell}} &= -J^{\text{f}}_{\text{water}}, \quad \text{at } x = x^{\text{f}}; \\ v_c - v_{\text{cell}} &= J^{\text{b}}_{\text{water}}, \quad \text{at } x = x^{\text{b}}, \end{aligned} \tag{3}$$

where J_{water} is the water influx across the cell membrane. Membrane water flux is driven by the combined hydrostatic and osmotic pressure difference of water across the cell membrane [12],

$$J^{\text{f(b)}}_{\text{water}} = -\alpha^{\text{f(b)}}\left[\left(p^{\text{f(b)}} - p^{\text{f(b)}}_*\right) - RT\left(c^{\text{f(b)}} - c^{\text{f(b)}}_0\right)\right], \tag{4}$$

where α is the permeability coefficient of water, c is the total concentration of all ion species (will be discussed later), R is the gas constant, and T is the absolute temperature. Due to the hydraulic resistance, the fluid pressure exerted on the outside of the cell, p_*, differs from the fluid pressure at infinity, p_∞. p_* can be solved as

$$p^{\text{f}}_* = p^{\text{f}}_\infty + d^{\text{f}}_g\left(v_{\text{cell}} - J^{\text{f}}_{\text{water}}\right),\; p^{\text{b}}_* = p^{\text{b}}_\infty - d^{\text{b}}_g\left(v_{\text{cell}} + J^{\text{b}}_{\text{water}}\right), \tag{5}$$

where $d^{\text{f(b)}}_g$ is the coefficient of external hydraulic resistance, which depends on the extracellular geometry and fluid viscosity. Approximated analytical expressions of $d^{\text{f(b)}}_g$ in the one-dimensional and three-dimensional spaces have been derived and computed in our prior work [27,31]. In this work, we will treat $d_g = d^{\text{f}}_g + d^{\text{b}}_g$ as a parameter. While d^{f}_g and d^{b}_g vary as cells move through the channel, the sum remains the same because the channel length is fixed. This coefficient of external hydraulic resistance determines whether cells can use water flux to drive cell migration. A large d_g enables cells to convert water flux into motility, whereas cells in a low d_g environment can only migrate via actomyosin dynamics [27,28].

C. Actin network mechanics

The F-actin forms a fluidlike actin network. The existence of the actin filament generates passive swelling stress, σ_n, which can be modeled by a linear constitutive relation, $\sigma_n = k_{\sigma_n}\theta_n$, where k_{σ_n} is the coefficient of actin swelling. A more involved constitutive relation from polymer physics can also be used [28]. Although we do not explicitly model the myosin in this work, the myosin contractile stress, σ_a, can still be included as a parameter if necessary. In this case, the total stress in the actin network will be $\sigma = \sigma_n - \sigma_a$. A model including myosin contractility can be found in our prior work [30].

The actin network connects to the extracellular matrix via focal adhesions [32]. As cells migrate, focal adhesions exert

an effective body force on the actin network in the opposite direction of the actin flow, v_n. The magnitude of the body force depends on the magnitude of the actin flow and the distribution of the actin network. It can be modeled by $\eta_{\rm st}\theta_n v_n$ [28,29], where $\eta_{\rm st}$ is the coefficient of focal adhesion, which depends on the substrate stiffness [33,34] and the size [35] and density [36] of adhesions. In this work, we treat $\eta_{\rm st}$ as a parameter and do not include the dynamics of focal adhesion [37].

The interfacial friction exerted on the cytosol also applies to the actin network. Putting all the forces together, we can write the force balance of the actin network,

$$-\frac{d\sigma}{dx} - \eta\theta_n(v_n - v_c) - \eta_{\rm st}\theta_n v_n = 0. \tag{6}$$

Since the actin network stress appears in the spatial derivative, the constant parameter of the myosin contractile stress, σ_a, does not influence the force balance of the actin network. For this reason, the current paper does not emphasize the role of myosin.

D. F-actin and G-actin exchange

Actin polymerization and depolymerization are essential processes in actin-driven cell migration. Polymerization typically occurs at the cell's front edge, whereas depolymerization occurs throughout the cytoplasm. Depolymerization can be considered a sink for F-actin but a source for G-actin. The amount of actin depolymerization per unit of time depends on the concentration of F-actin, which can be represented by $\gamma\theta_n$, where γ is the rate of actin depolymerization. Thus the material balance for F-actin and G-actin are

$$\frac{d}{dx}(\theta_n v_n) = -\gamma\theta_n, \tag{7}$$

$$\frac{d}{dx}(\theta_c v_c) = D_{\theta_c}\frac{d^2}{dx^2}\theta_c + \gamma\theta_n, \tag{8}$$

where D_{θ_c} is the diffusion coefficient of G-actin in the cytosol.

The contribution of actin polymerization is modeled through flux boundary conditions of Eqs. (7) and (8). At the front of the cell, the flux boundary conditions for F-actin and G-actin are

$$\theta_n(v_n - v_{\rm cell})|_{x=x^{\rm f}} = -J^{\rm f}_{\rm actin},$$
$$\left[-D_{\theta_c}\frac{d\theta_c}{dx} + \theta_c(v_c - v_{\rm cell})\right]\Big|_{x=x^{\rm f}} = J^{\rm f}_{\rm actin}, \tag{9}$$

where $J^{\rm f}_{\rm actin}$ is the rate of actin polymerization. We assume that the rate of actin polymerization increases with the concentration of G-actin, θ_c, and saturates when θ_c is large. Therefore $J^{\rm f}_{\rm actin}$ takes the form

$$J^{\rm f}_{\rm actin} = J_a\frac{\theta^{\rm f}_c}{\theta_{c,c} + \theta^{\rm f}_c}, \tag{10}$$

where J_a is the coefficient of actin polymerization and $\theta_{c,c}$ is a constant. $\theta^{\rm f}_c$ is the concentration of G-actin at the front of the cell, i.e., $\theta^{\rm f}_c = \theta_c|_{x=x^{\rm f}}$. Since there is no polymerization at the back of the cell, the fluxes for F-actin and G-actin are zero at $x = x^{\rm b}$,

$$\theta_n(v_n - v_{\rm cell})|_{x=x^{\rm f}} = 0,$$
$$\left[-D_{\theta_c}\frac{d\theta_c}{dx} + \theta_c(v_c - v_{\rm cell})\right]\Big|_{x=x^{\rm f}} = 0. \tag{11}$$

Within the time scale of consideration, the total amount of actin is conserved so that the average concentration of actin, θ_*, should be a constant, i.e.,

$$\int_{x^{\rm b}}^{x^{\rm f}}(\theta_n + \theta_c)dx = L\theta_*. \tag{12}$$

In the model, θ_* is prescribed but θ_c and θ_n are solved.

E. Solute species and osmolarity

The boundary condition of the cytosol involves membrane water flux [Eq. (4)] as a function of the total solute concentration. The solutes are essential because they determine the osmotic pressure and specify the pH and electric potential. We include in the model the ion species most abundant in cells (such as sodium, potassium, and chloride) and are crucial to studying the pH (i.e., hydrogen) and electric potential. We cannot neglect the concentration of bicarbonate if hydrogen is included because of the bicarbonate-carbonic acid pair reaction.

Within the cell, we consider the following solute species: Na^+, K^+, Cl^-, H^+, HCO_3^-, A^-, Buf^-, and HBuf. A^- is the nonpermeable large molecules or proteins, which we assume has valence -1, Buf^- is a generic deprotonated buffer species, and HBuf is the corresponding protonated buffer species. So the intracellular solute concentration space is $c_i = \{c_{\rm Na}, c_{\rm K}, c_{\rm Cl}, c_{\rm H}, c_{\rm HCO_3}, c_{\rm A}, c_{\rm Buf}, c_{\rm HBuf}\}^{\rm T}$. Outside of the cell, we neglect the buffer solution but include an electroneutral, nonpermeable solute, G. An example of such a solute is glucose. So the extracellular solute concentration space is $c^{\rm f(b)}_{i,0} = \{c^{\rm f(b)}_{\rm Na,0}, c^{\rm f(b)}_{\rm K,0}, c^{\rm f(b)}_{\rm Cl,0}, c^{\rm f(b)}_{\rm H,0}, c^{\rm f(b)}_{\rm HCO_3,0}, c^{\rm f(b)}_{\rm A,0}, c^{\rm f(b)}_{\rm G,0}\}^{\rm T}$. Here we allow the extracellular solute concentration to be different at the two ends of the cell. In this work, we do not calculate the ion diffusion in the extracellular space. The concentrations c_0's refer to the extracellular ion concentrations on the cell boundary directly sensed by the cell.

The c and c_0 in Eq. (4) are defined by

$$c = \sum c_i, \quad c^{\rm f(b)}_0 = \sum c^{\rm f(b)}_{i,0}, \tag{13}$$

which are the osmolarities inside and outside of the cell.

F. Chemical reactions and pH

We consider two types of chemical reactions in the model: the bicarbonate-carbonic acid pair and the buffer pair. The chemical equilibrium equation for the bicarbonate-carbonic acid pair is

$$CO_2(aq) + H_2O(l) \rightleftharpoons H^+(aq) + HCO_3^-(aq), \tag{14}$$

where $[CO_2]_{\rm aq}$ is related to the partial pressure of CO_2, P_{CO_2}, by the Henry constant k_H, $[CO_2]_{\rm aq} = P_{CO_2}/k_H$. The reaction equilibrium constant is

$$k_c = \frac{[HCO_3^-]_{\rm aq}[H^+]_{\rm aq}}{[CO_2]_{\rm aq}}. \tag{15}$$

We let $\mathrm{pH}_0 = -\log_{10}[\mathrm{H}^+]_{\mathrm{aq},0}$ as the extracelluar pH and $\mathrm{p}K_c = -\log_{10}k_c$ so that Eq. (15) becomes

$$\mathrm{pH}_0 - \mathrm{p}K_c = \log_{10}\frac{[\mathrm{HCO}_3^-]^0_{\mathrm{aq}}}{P_{\mathrm{CO}_2}/k_H}. \tag{16}$$

$[\mathrm{CO}_2]_{\mathrm{aq}} = [\mathrm{CO}_2]^0_{\mathrm{aq}}$ since CO_2 can move freely across the cell membrane [21]. Once the extracellular concentration of bicarbonate and the partial pressure of CO_2 are given, the extracellular pH is also uniquely determined. Similarly, in the intracellular domain, we have

$$\mathrm{pH} - \mathrm{p}K_c = \log_{10}\frac{[\mathrm{HCO}_3^-]_{\mathrm{aq}}}{[\mathrm{CO}_2]_{\mathrm{aq}}}, \tag{17}$$

where $\mathrm{pH} = -\log_{10}[\mathrm{H}^+]_{\mathrm{aq}}$ is the intracelluar pH. The chemical reaction for the intracellular buffer solution is

$$\mathrm{HBuf(aq)} \rightleftharpoons \mathrm{H}^+\mathrm{(aq)} + \mathrm{Buf}^-\mathrm{(aq)}. \tag{18}$$

The reaction equilibrium constant is similarly $k_B = [\mathrm{Buf}^-]_{\mathrm{aq}}[\mathrm{H}^+]_{\mathrm{aq}}/[\mathrm{HBuf}]_{\mathrm{aq}}$. With $\mathrm{p}K_B = -\log_{10}k_B$, we have

$$\mathrm{pH} - \mathrm{p}K_B = \log_{10}\frac{[\mathrm{Buf}^-]_{\mathrm{aq}}}{[\mathrm{HBuf}]_{\mathrm{aq}}}. \tag{19}$$

A model with a more involved buffer solution reaction has been considered where the valance of the deprotonated buffer can take on any numbers [38]. However, this will not affect our model prediction.

Since we assume that the buffer solution only exists inside the cell, it is equivalent to saying that the buffer solutes are nonpermeable. The total amount of nonpermeable solutes is conserved within the cell so that

$$S\int_{x^{\mathrm{b}}}^{x^{\mathrm{f}}} c_A dx = N_A, \quad S\int_{x^{\mathrm{b}}}^{x^{\mathrm{f}}} (c_{\mathrm{Buf}} + c_{\mathrm{HBuf}})dx = N_{\mathrm{Buf}} + N_{\mathrm{HBuf}}, \tag{20}$$

where S is the cross-sectional area of the cell, N_A is the total amount of intracellular nonpermeable large molecules, and $N_{\mathrm{Buf}} + N_{\mathrm{HBuf}}$ is the total amount of buffer solutes inside the cell. Both N_A and $N_{\mathrm{Buf}} + N_{\mathrm{HBuf}}$ are given parameters in the model.

With all the relations established above, we can express the concentrations of hydrogen, bicarbonate, and protonated buffer solute as functions of the primary variables [Eq. (1)], i.e.,

$$c_{\mathrm{H}}(x) = 10^3 10^{-\mathrm{pH}}, \quad c_{\mathrm{HCO}_3}(x) = \frac{P_{\mathrm{CO}_2}}{k_H}10^{\mathrm{pH}-\mathrm{p}K_c},$$
$$c_{\mathrm{HBuf}}(x) = c_{\mathrm{Buf}}10^{\mathrm{p}K_B-\mathrm{pH}}, \tag{21}$$

which should be satisfied at all points in space.

G. Ion dynamics

Diffusion, convection, and electric drift happen for each solute species in the cytosol. The flux for each species is

$$J_i = -D_i\frac{dc_i}{dx} + v_c c_i - D_i\frac{z_i F}{RT}c_i\frac{d\phi}{dx},$$
$$i \in \{\mathrm{Na}^+, \mathrm{K}^+, \mathrm{Cl}^-, \mathrm{H}^+, \mathrm{HCO}_3^-, \mathrm{A}^-, \mathrm{Buf}^-, \mathrm{HBuf}\}, \tag{22}$$

where c_i, z_i, and D_i are, respectively, each solute species' concentration, valance, and diffusion constant (note that $z_{\mathrm{HBuf}} = 0$). ϕ is the intracellular electric potential. F, R, and T are Faraday's constant, ideal gas constant, and absolute temperature, respectively.

The governing equations and boundary conditions for c_{Na}, c_{K}, c_{Cl}, and c_{A}, which are nonreactive species, are

$$-\frac{dJ_{\mathrm{Na}}}{dx} = 0, \quad J_{\mathrm{Na}}|_{x=x^{\mathrm{f}}} = -J^{\mathrm{f}}_{\mathrm{Na}}, \quad J_{\mathrm{Na}}|_{x=x^{\mathrm{b}}} = J^{\mathrm{b}}_{\mathrm{Na}}, \tag{23}$$
$$-\frac{dJ_{\mathrm{K}}}{dx} = 0, \quad J_{\mathrm{K}}|_{x=x^{\mathrm{f}}} = -J^{\mathrm{f}}_{\mathrm{K}}, \quad J_{\mathrm{K}}|_{x=x^{\mathrm{b}}} = J^{\mathrm{b}}_{\mathrm{K}}, \tag{24}$$
$$-\frac{dJ_{\mathrm{Cl}}}{dx} = 0, \quad J_{\mathrm{Cl}}|_{x=x^{\mathrm{f}}} = -J^{\mathrm{f}}_{\mathrm{Cl}}, \quad J_{\mathrm{Cl}}|_{x=x^{\mathrm{b}}} = J^{\mathrm{b}}_{\mathrm{Cl}}, \tag{25}$$
$$-\frac{dJ_{\mathrm{A}}}{dx} = 0, \quad J_{\mathrm{A}}|_{x=x^{\mathrm{f}}} = J_{\mathrm{A}}|_{x=x^{\mathrm{b}}} = 0, \tag{26}$$

where the boundary fluxes are positive inwards. The governing equations for reactive species, such as the hydrogen ions, the bicarbonate, and the buffer solutions, should be treated differently because of the chemical reactions in Eqs. (14) and (18). Instead of using $dJ_i/dx = 0$ for each reactive species as in Eqs. (23)–(26), we need to consider the conservation of total species from the two chemical reactions. The governing equation and boundary conditions for pH, i.e., c_{H}, are

$$-\frac{d}{dx}\left(J_{\mathrm{HCO}_3} + J_{\mathrm{Buf}} - J_{\mathrm{H}}\right) = 0,$$
$$\left(J_{\mathrm{HCO}_3} + J_{\mathrm{Buf}} - J_{\mathrm{H}}\right)\big|_{x=x^{\mathrm{f}}} = -\left(J^{\mathrm{f}}_{\mathrm{HCO}_3} + J^{\mathrm{f}}_{\mathrm{Buf}} - J^{\mathrm{f}}_{\mathrm{H}}\right),$$
$$\left(J_{\mathrm{HCO}_3} + J_{\mathrm{Buf}} - J_{\mathrm{H}}\right)\big|_{x=x^{\mathrm{b}}} = \left(J^{\mathrm{b}}_{\mathrm{HCO}_3} + J^{\mathrm{b}}_{\mathrm{Buf}} - J^{\mathrm{b}}_{\mathrm{H}}\right). \tag{27}$$

where $J^{\mathrm{b/f}}_{\mathrm{Buf}} = 0$ due to the assumed nonpermeability of buffer solutions. The governing equation and boundary conditions for c_{Buf} are

$$-\frac{d}{dx}(J_{\mathrm{Buf}} + J_{\mathrm{HBuf}}) = 0,$$
$$(J_{\mathrm{Buf}} + J_{\mathrm{HBuf}})|_{x=x^{\mathrm{f}}} = (J_{\mathrm{Buf}} + J_{\mathrm{HBuf}})|_{x=x^{\mathrm{b}}} = 0. \tag{28}$$

Equations (27) and (28) are equivalent to incorporating reaction terms in the diffusion-reaction-advection equations for the reactive species. The combination of the reaction terms vanishes upon the conservation law.

The intracellular electric potential is solved by the electroneutrality condition, i.e.,

$$\sum z_i c_i = 0. \tag{29}$$

The same condition is also imposed outside the cell when we set up the parameters for extracellular solute concentrations. This electroneutrality condition enforces that the net charge is 0 everywhere, leading to $\nabla^2\phi = 0$. We thus know that the intracellular voltage is a linear function in space, i.e., $\nabla\phi = \mathrm{const}$. Therefore Eq. (22) can be written as

$$J_i = -D_i\frac{dc_i}{dx} + \left(v_c - D_i\frac{z_i F}{RT}\frac{d\phi}{dx}\right)c_i. \tag{30}$$

The term in the parentheses is a constant, meaning that the combined cytosol flow and electric drift generate an effective convection velocity for each solute species. The relative

contribution of each flux mechanism can be analyzed by approximating individual terms. The diffusive flux is $J_{i,\mathrm{diff}} \approx -D_i(c_i^{\mathrm{f}} - c_i^{\mathrm{b}})/L$, the convective flux is $J_{i,\mathrm{conv}} \approx v_c(c_i^{\mathrm{f}} + c_i^{\mathrm{b}})/2$, and the electric drift flux is $J_{i,\mathrm{drif}} \approx -D_i z_i F(\phi^{\mathrm{f}} - \phi^{\mathrm{b}})(c_i^{\mathrm{f}} + c_i^{\mathrm{b}})/(2RTL)$. The amplitude and gradient of the ion concentrations vary among different ion species. Therefore the relative significance of each term also varies. When the intracellular electric potential gradient is negligible, the contribution from the electric drift is also expected to be negligible.

Note that the ion dynamics described in this section is generic, meaning that these are intracellular fluxes and are independent of the choice of membrane ion channels, transporters, and pumps, which we discuss next.

H. Ion channels, transporters, and pumps

To specify the boundary ion fluxes for each species, $J_i^{\mathrm{b/f}}$, the ion channels, transporters, and pumps need to be modeled. In this work, we choose the following membrane carriers: passive Na^+ channel, passive K^+ channel, passive Cl^- channel (including SWELL1), Na^+/K^+ pump (NKE), Na^+/H^+ exchanger (NHE), and Cl^-/HCO_3^- exchanger (AE2).

The passive ion fluxes, $J_{i,p}^{\mathrm{f(b)}}$, are proportional to the electrochemical potential difference of ions across the membrane [39],

$$J_{i,p}^{\mathrm{f(b)}} = \alpha_{i,p}^{\mathrm{f(b)}} G_m^{\mathrm{f(b)}} \left[RT \ln \Gamma_i^{\mathrm{f(b)}} - z_i F\left(\phi^{\mathrm{f(b)}} - \phi_0^{\mathrm{f(b)}}\right)\right], \quad i \in \{\mathrm{Na}^+, \mathrm{K}^+, \mathrm{Cl}^-\}, \tag{31}$$

where $\Gamma_i^{\mathrm{f(b)}} = c_{i,0}^{\mathrm{f(b)}}/c_i^{\mathrm{f(b)}}$ is the ratio of extra- to intracellular ion concentrations at the two ends of the cell; $\alpha_{i,p}^{\mathrm{f(b)}}$ is the permeability coefficient of each species, which depends on the channel property and the density of the channels in the membrane. The factor $G_m^{\mathrm{f(b)}} \in (0, 1)$ is a mechanosensitive gating function representing the probability of channel opening. Considering that the passive channels are typically tension-gated [40], we let $G_m^{\mathrm{f(b)}} = [1 + e^{-\beta_\tau(\tau_m^{\mathrm{f(b)}} - \tau_{m,c})}]^{-1}$, where β_τ and $\tau_{m,c}$ are two constants and $\tau_m^{\mathrm{f(b)}}$ is the cortical (combine with the membrane) tension on either end of the cell. The cortical tension can be calculated from the force balance at the two ends of the cell,

$$\tau_m^{\mathrm{f(b)}} = \frac{w}{2}\left(\sigma^{\mathrm{f(b)}} + p_c^{\mathrm{f(b)}} - p_*^{\mathrm{f(b)}}\right), \tag{32}$$

where w is the width of the cell. Such defined distribution, G_m, indicates that the probability of passive channel opening increases with increasing cortical tension. The numerical calculation shows that in this work the passive channels are fully open.

The Na^+/K^+ pump (NKE) is a ubiquitous and vital active ion pump that maintains the membrane potential of cells. It exports three Na^+ ions and intakes two K^+ ions per ATP molecule. Because the overall flux is positive outwards, the pump's activity depends on the membrane potential [41]. The NKE flux also depends on the concentrations of Na^+ and K^+ [42,43] and saturates at high concentration limits [43]. Based on these facts, we model the flux of Na^+ and K^+ through the Na^+/K^+ pump as

$$J_{\mathrm{NKE}}^{\mathrm{f(b)}} = J_{\mathrm{NKE,Na}}^{\mathrm{f(b)}} = -\frac{3}{2} J_{\mathrm{NKE,K}}^{\mathrm{f(b)}} = -\frac{\alpha_{\mathrm{NKE}}^{\mathrm{f(b)}} G_{V,\mathrm{NKE}}^{\mathrm{f(b)}}}{\left(1 + \beta_{\mathrm{NKE,Na}}\Gamma_{\mathrm{Na}}^{\mathrm{f(b)}}\right)^3 \left(1 + \beta_{\mathrm{NKE,K}}/\Gamma_{\mathrm{K}}^{\mathrm{f(b)}}\right)^2}, \tag{33}$$

where $\alpha_{\mathrm{NKE}}^{\mathrm{f(b)}}$ is the permeability coefficient of the pump depending on the density of the pump as well as the concentration of ATP. $\beta_{\mathrm{NKE,Na}}$ and $\beta_{\mathrm{NKE,K}}$ are constants that scale $\Gamma_{\mathrm{Na}}^{\mathrm{f(b)}}$ and $\Gamma_{\mathrm{K}}^{\mathrm{f(b)}}$, respectively. These two constants are intrinsic properties of the Na^+/K^+ pump and, thus, do not differ at the two ends of the cells. The exponents 3 and 2 are Hill's coefficients of Na^+ and K^+, respectively. Equation (33) ensures that the flux is zero when either $1/\Gamma_{\mathrm{Na}}^{\mathrm{f(b)}}$ or $\Gamma_{\mathrm{K}}^{\mathrm{f(b)}}$ approaches zero; the flux saturates if $1/\Gamma_{\mathrm{Na}}^{\mathrm{f(b)}}$ and $\Gamma_{\mathrm{K}}^{\mathrm{f(b)}}$ approaches infinity. $G_{V,\mathrm{NKE}}^{\mathrm{f(b)}}$ captures the voltage-dependence of the pump activity [41], $G_{V,\mathrm{NKE}}^{\mathrm{f(b)}} = 2[1 + e^{-\beta_\phi(\phi^{\mathrm{f(b)}} - \phi_c)}]^{-1} - 1$, where β_ϕ and ϕ_c are constants that reflects the intrinsic voltage-gating property of NKE.

The Na^+/H^+ exchanger (NHE), which has ten identified isoforms, is expressed in almost all tissues [21]. It imports one Na^+ and extrudes one H^+ under physiological conditions. This exchanger has significant effects on water flux, cell volume regulation [44–49], cell migration [14,50–52], and is a major therapeutic target [21,53,54]. NHE is quiescent at intracellular pH > 7.2 [55]. The flux of NHE can thus be expressed as

$$J_{\mathrm{NHE}}^{\mathrm{f(b)}} = J_{\mathrm{NHE,Na}}^{\mathrm{f(b)}} = -J_{\mathrm{NHE,H}}^{\mathrm{f(b)}} = \alpha_{\mathrm{NHE}}^{\mathrm{f(b)}} G_{\mathrm{NHE}}^{\mathrm{f(b)}} RT\left(\ln \Gamma_{\mathrm{Na}}^{\mathrm{f(b)}} - \ln \Gamma_{\mathrm{H}}^{\mathrm{f(b)}}\right), \tag{34}$$

where $\alpha_{\mathrm{NHE}}^{\mathrm{f(b)}}$ is the permeability coefficient which does not significantly depend on cortical tension [56]. However, $\alpha_{\mathrm{NHE}}^{\mathrm{f(b)}}$ depends on the density of membrane NHE, which is affected by multiple factors, including the presence of F-actin on the cell membrane [16,21]. $G_{\mathrm{NHE}}^{\mathrm{f(b)}} = [1 + e^{\beta_{\mathrm{NHE}}(\mathrm{pH}^{\mathrm{f(b)}} - \mathrm{pH}_{\mathrm{NHE},c})}]^{-1}$ is a pH-gated function indicating the dependence of the NHE activity on pH. β_{NHE} and $\mathrm{pH}_{\mathrm{NHE},c}$ are two constants reflecting the NHE properties.

The Cl^-/HCO_3^- exchanger (AE2), which imports one Cl^- and extrudes one HCO_3^-, is also common in cells. This exchanger is almost quiescent at intracellular pH < 6.8–7.3. Similarly, we assume that the flux takes the form

$$J_{\mathrm{AE2}}^{\mathrm{f(b)}} = J_{\mathrm{AE2,Cl}}^{\mathrm{f(b)}} = -J_{\mathrm{AE2,HCO_3}}^{\mathrm{f(b)}} = \alpha_{\mathrm{AE2}}^{\mathrm{f(b)}} G_{\mathrm{AE2}}^{\mathrm{f(b)}} RT\left(\ln \Gamma_{\mathrm{Cl}}^{\mathrm{f(b)}} - \ln \Gamma_{\mathrm{HCO_3}}^{\mathrm{f(b)}}\right), \tag{35}$$

where $\alpha_{\mathrm{AE2}}^{\mathrm{f(b)}}$ is the permeability coefficient of AE2 and is assumed to be independent of the cortical tension. $G_{\mathrm{AE2}}^{\mathrm{f(b)}} = [1 + e^{-\beta_{\mathrm{AE2}}(\mathrm{pH}^{\mathrm{f(b)}} - \mathrm{pH}_{\mathrm{AE2},c})}]^{-1}$ is a pH-gated function indicating the dependence of the AE2 activity on pH. β_{AE2} and $\mathrm{pH}_{\mathrm{AE2},c}$ are two constants reflecting the AE2 properties.

With all these ion carriers considered, the boundary fluxes for each ion species are:

$$J_{\mathrm{Na}}^{\mathrm{f(b)}} = J_{\mathrm{Na},p}^{\mathrm{f(b)}} + J_{\mathrm{NKE,Na}}^{\mathrm{f(b)}} + J_{\mathrm{NHE,Na}}^{\mathrm{f(b)}}, \tag{36}$$

$$J_{\mathrm{K}}^{\mathrm{f(b)}} = J_{\mathrm{K},p}^{\mathrm{f(b)}} + J_{\mathrm{NKE,K}}^{\mathrm{f(b)}}, \tag{37}$$

$$J_{\mathrm{Cl}}^{\mathrm{f(b)}} = J_{\mathrm{Cl},p}^{\mathrm{f(b)}} + J_{\mathrm{AE2,Cl}}^{\mathrm{f(b)}}, \tag{38}$$

$$J_{\mathrm{H}}^{\mathrm{f(b)}} = J_{\mathrm{NHE,H}}^{\mathrm{f(b)}}, \tag{39}$$

$$J_{\mathrm{HCO_3}}^{\mathrm{f(b)}} = J_{\mathrm{AE2,HCO_3}}^{\mathrm{f(b)}}. \tag{40}$$

I. Force balance of the cell

At the back of the cell, F-actin adheres to the substrate through transmembrane proteins (integrins), which provide an adhesive force, $F_{\mathrm{ad}}^{\mathrm{b}}$, that resists cell migration. We let the adhesive force be proportional to the cell velocity, i.e., $F_{\mathrm{ad}}^{\mathrm{b}} = k_{\mathrm{ad}} v_{\mathrm{cell}}$, where k_{ad} is the coefficient of adhesive force. This adhesive force is equivalent to the effective frictional force between the cell and the substrate.

To establish a force balance relation of the cell, we can draw a free-body diagram of the cell and collect all the forces applied to the cell either from the extracellular matrix or through other external means. Any internal forces within the cell should be excluded when analyzing a free-body diagram. This condition also means the choices of the constitutive relations for the actin network, such as actin swelling and myosin contraction, do not affect the force balance of the cell.

Putting together, the force balance of the entire cell is

$$-(p_*^{\mathrm{f}} - p_*^{\mathrm{b}}) - \eta_{\mathrm{st}} \int_{x^{\mathrm{b}}}^{x^{\mathrm{f}}} \theta_n v_n dx - k_{\mathrm{ad}} v_{\mathrm{cell}} = 0, \tag{41}$$

where p_*'s are defined in Eq. (5).

The primary variables [Eq. (1)] are numerically solved by solving all the coupled nonlinear equations and boundary conditions. The one-dimensional space is discretized into elements where the finite difference method is applied. The discretized equations are solved with the Newton-Raphson iteration scheme. Other variables are expressed in terms of the unknowns or are considered model parameters.

J. Coupling between mechanics and chemistry

We now extend the prior model to include additional couplings between the mechanical and biochemical parts of the model. Specifically, we let pH and NHE be coupled with the actin network [red arrows in Fig. 1(c)]. This effort is achieved through two parallel schemes.

The rate of actin depolymerization, γ, depends on multiple mechanical and biochemical factors [57]. One of the factors we are considering here is pH [58]. Experimental data suggests that higher pH leads to a higher rate of actin depolymerization [58]. We thus let

$$\gamma = \gamma_0 + \frac{\gamma_{\mathrm{pH}}}{1 + e^{-\beta_\gamma(\mathrm{pH} - \mathrm{pH}_{\gamma,c})}}, \tag{42}$$

where γ_0 is a baseline rate of actin depolymerization, and γ_{pH} is the coefficient of pH-dependent rate of actin depolymerization. β_γ and $\mathrm{pH}_{\gamma,c}$ are two constants characterizing the slope and value, respectively, of the inflection point of γ as a function of pH. The biophysical interpretation of each parameter is illustrated in Fig. 1(d). Note that pH is a function of space x, so γ is also a spatial function.

Our recent work showed that the expression of NHE is coupled to F-actin density [16], a mechanism controlled by a protein known as ezrin [21]. In this work, we will study, from a theoretical point of view, how this coupling affects cell homeostasis and migration. Since the membrane expression of NHE decreases with decreasing F-actin presence, we let the permeability coefficient of NHE be a function of F-actin concentration

$$\alpha_{\mathrm{NHE}}^{\mathrm{f(b)}} = \alpha_{\mathrm{NHE,F}}^{\mathrm{f(b)}} \left[1 + e^{-\beta_F(\theta_n^{\mathrm{f(b)}}/\theta_{n,*} - \beta_{F,c})}\right]^{-1}, \tag{43}$$

where $\alpha_{\mathrm{NHE,F}}^{\mathrm{f(b)}}$ is the maximum permeability coefficient, which depends on cell types and other transcription factors. β_F and $\beta_{F,c}$ are constants controlling the slope and value, respectively, of the inflection point of α_{NHE} as a function of the ratio $\theta_n^{\mathrm{f(b)}}/\theta_{n,*}$. The biophysical interpretation of each parameter is illustrated in Fig. 1(d). When the actin dependence of NHE permeability is muted, we will let $\alpha_{\mathrm{NHE}}^{\mathrm{f(b)}} = \alpha_{\mathrm{NHE,F}}^{\mathrm{f(b)}} = \mathrm{conts.}$, which can be different at the two ends of the cell.

K. Model summary

The model is tightly coupled [Fig. 1(c)]; no equation can be solved individually without solving all the other equations. Here, we summarize how different components of the model couple together. The cytosol mechanics (Sec. II B) is an integral part of the model, affecting all the other processes. From the kinetics aspect, the cytosol flow and the F-actin flow create an interfacial stress that acts on both the cytosol and the actin network phases [Eqs. (2) and (6)]. The cytosol pressure enters into the chemical potential of water [Eq. (4)], the force balance of the membrane/cortex [Eq. (32)], and the force balance of the cell [Eq. (41)]. From the kinematics aspect, the cytosol velocity affects the boundary motion of the cell [Eq. (3)] and provides the advection driving force for the G-actin [Eq. (8)] and solutes [Eq. (22)].

Among the actin molecules, the F-actin and G-actin interconvert through polymerization [J_{actin}, Eqs. (9) and (10)] and depolymerization [γ, Eqs. (7) and (8)]. F-actin concentration and velocity govern the force from focal adhesion [Eq. (6)], which is reflected in the cell balance and velocity [Eq. (41)]. In this new model, the actin dynamics is further coupled to the rest of the system through pH [Eq. (42)] and NHE-ezrin]Eq. (43)] [Fig. 1(c), red arrows]. This coupling is a mathematical reflection of mechanical and biochemical interaction in a cellular system.

The cellular osmolarity is the key quantity that influences water flux across the membrane [Eq. (4)]. The total osmolarity is a combination of the concentrations of various ion species and solutes [Eq. (13)]. The concentration of each ion species results from all relevant ion carriers (Sec. II H). The membrane potential, ϕ, not only affects the passive fluxes [Eq. (31)] but is also a result of the electroneutrality condition [Eq. (29)]. The intracellular pH is central to the chemical reactions [Eqs. (14) and (18)], which couple to the rest of the solutes via the sodium-hydrogen exchanger (NHE) [Eq. (34)]. Meanwhile, the membrane potential and intracellular pH serve as gating functions in multiple ion carriers.

TABLE I. Model parameters on the mechanical part.

Parameter	Description	Value	Source
R (J/(mol K))	Ideal gas constant	8.31	Physical constant
T (K)	Absolute temperature	310	Physiological condition
L (μm)	Cell length	50	Based on Ref. [15]
w (μm)	Cell width	3	Based on Ref. [15]
η (Pa s/(μm^2 mM))	Drag coefficient between two phases	10^{-2}	Based on Ref. [60]
$\eta_{\rm st}$ (Pa s/(μm^2 mM))	Coefficient of drag from focal adhesion	10^2	Based on Refs. [15,30]
k_{σ_n} (Pa/mM)	Coefficient of the passive F-actin stress	10^2	Based on Refs. [15,30]
$k_{\rm ad}$ (Pa s/μm)	Coefficient in $F^{\rm b}_{\rm ad} = k_{\rm ad} v_{\rm cell}$	300	Based on Refs. [15,30]
d_g (Pa s/μm)	Coefficient of hydraulic pressure	20	Ref. [15]
D_{θ_c} (μm^2/s)	Diffusion coefficient of G-actin	10	Refs. [61–64]
θ_* (mM)	Average concentration of total actin	0.3	Based on Refs. [65,66]
J_a (nm mM/s)	Coefficient in $J^{\rm f}_{\rm actin} = J_a \theta^{\rm f}_c/(\theta_{c,c} + \theta^{\rm f}_c)$	6	Ref. [30]
$\theta_{c,c}$ (μM)	Critical value of actin polymerization	0.2	Ref. [66]
γ_0 (1/s)	Baseline rate of actin depolymerization	10^{-3}	Based on Ref. [30]
$\gamma_{\rm pH}$ (1/s)	Coefficient of pH-dependent rate of actin depolymerization	2×10^{-3}	Estimated
β_γ	Constant in γ	15	Estimated
$\rm pH_{\gamma,c}$	Constant in γ	7.38	Estimated
p_∞ (Pa)	External pressure at the front and back	0	Free parameter

The 13 primary variables in the model [Eq. (1)] correspond to 13 governing equations and their respective boundary conditions, all solved simultaneously. We summarize the nominal governing equations and the boundary conditions for each variable in the table below.

Variables	Nominal governing equations	Nominal boundary conditions
$p(x)$	Eq. (2) (the first relation)	Eq. (3) (the first relation)
v_c	Eq. (2) (the second relation)	Eq. (3) (the second relation)
$v_n(x)$	Eq. (6)	Eq. (9) (the first relation)
$\theta_n(x)$	Eq. (7)	Eq. (9) (the first relation)
$\theta_c(x)$	Eq. (8)	Eq. (11) (the second relation) and Eq. (12)
$c_{\rm Na}(x)$	Eq. (23)	Eq. (23)
$c_{\rm K}(x)$	Eq. (24)	Eq. (24)
$c_{\rm Cl}(x)$	Eq. (25)	Eq. (25)
$\rm pH(x)$	Eq. (27)	Eq. (27)
$c_{\rm A}(x)$	Eq. (26)	Eq. (26)
$c_{\rm Buf}(x)$	Eq. (28)	Eq. (28)
$\phi(x)$	Eq. (29)	N/A
$v_{\rm cell}$	Eq. (41)	N/A

Equation (8) is a second-order differential equation and requires two boundary conditions. It is tempting to use Eq. (9) (the second relation) and Eq. (11) (the second relation) as the two conditions. However, the four relations in Eqs. (9) and (11) are not linearly independent, as evident when adding Eqs. (7) and (8) together. Therefore one of the four boundary conditions should be replaced by a condition specifying the total amount of actin within a cell.

L. Model parameters

All the parameters used in the model are listed in Tables I and II. We have divided the parameter tables into a mechanical part and an electrochemical part to highlight that our model is a meaningful synthesis of advanced mechanical models of cell migration [27–29] and involves an electrochemical model of cell homeostasis [38,59]. In the mechanical part, the parameters are chosen to ensure that the model generates robust and stable mechanical interactions between actin and cytosol while predicting cell velocity within the range typical of a mammalian cell. In the electrochemical part, the chosen parameters, in particular the ion carrier permeability and chemical reaction equilibrium constants, represent typical mammalian tissue cells under physiological conditions, ensuring that they generate pH, membrane potential, and ion concentrations within expected physiological ranges [38].

Significant deviations from the current parameters will result in dysregulated intracellular pH, membrane potential, and ion concentrations. We will demonstrate some of these dysregulated states in the results. However, small perturbations of the parameters will not lead to a significant departure from the expected homeostasis. For example, in this study, we perturb the polarization ratio of several ion carriers, and the predicted cell behaviors remain within the expected ranges. Cells in pathological conditions require a different parameter set. Given the potential variation from cell type to cell type, we do not focus on the particular results or numbers predicted by the model. Rather, we emphasize the mechanisms behind why the model predicts certain trends of cellular dynamics as functions of solute carrier polarizations, which can be observed in experiments via antibodies targeting specific carriers.

When we show results from polarization ion carriers, we specify the polarization ratio as the ratio of ion permeability at the front to the rate at the back. The average permeability will remain the same as those listed in Table II while the front and

TABLE II. Model parameters on the electrochemical part.

Parameter	Description	Value	Source
N_A (pmol)	Total intracellular A^-	7×10^{-2}	Based on Ref. [15]
$N_{\text{Buf}} + N_{\text{HBuf}}$ (pmol)	Total intracellular Buffer Solution	7×10^{-2}	Based on Ref. [15]
α_w (nm/(Pa s))	Permeability coefficient of water	0.1	Ref. [67]
$\alpha_{\text{Na},p}$ (mol^2/(J μm^2 s))	Permeability of Na	0.1	Based on Refs. [15,38]
$\alpha_{\text{K},p}$ (mol^2/(J μm^2 s))	Permeability of K	1.5×10^2	Based on Refs. [15,38]
$\alpha_{\text{Cl},p}$ (mol^2/(J μm^2 s))	Permeability of Cl	10^2	Based on Refs. [15,38]
α_{NKE} (mol/(μm^2 s))	Permeability of NKE	3.9×10^3	Based on Refs. [15,38]
$\alpha_{\text{NHE,F}}$ (mol^2/(J μm^2 s))	Permeability of NHE	10^3	Based on Refs. [15,38]
α_{AE2} (mol^2/(J μm^2 s))	Permeability of AE2	5×10^2	Based on Refs. [15,38]
D_i (μm^2/s)	Diffusion coefficient of each ion species	100	Based on Refs. [14,68,69][a]
$\beta_{\text{NKE,Na}}$	Constant in J_{NKE}	0.1	Based on Refs. [15,38]
$\beta_{\text{NKE,K}}$	Constant in J_{NKE}	0.01	Based on Refs. [15,38]
β_τ (m/N)	Constant in G_m	2×10^3	Based on Refs. [15,38]
$\tau_{m,c}$ (N/m)	Constant in G_m	5×10^{-4}	Based on Refs. [15,38]
β_ϕ (1/mV)	Constant in $G_{V,\text{NKE}}$	0.03	Ref. [41]
ϕ_c (mV)	Constant in $G_{V,\text{NKE}}$	−150	Ref. [41]
β_{NHE}	Constant in G_{NHE}	15	Ref. [55]
$\text{pH}_{\text{NHE},c}$	Constant in G_{NHE}	7.2	Ref. [55]
β_{AE2}	Constant in G_{AE2}	10	Ref. [55]
$\text{pH}_{\text{AE2},c}$	Constant in G_{AE2}	7.1	Ref. [55]
β_F	Constant in α_{NHE}	5	Estimated
$\beta_{F,c}$	Constant in α_{NHE}	0.1	Estimated
k_H (atm/M)	Henry's constant	29	Ref. [70]
P_{CO_2} (atm)	Partial pressure of CO_2	5%	Physiological condition
$\text{p}K_c$	pK for bicarbonate-carbonic acid pair	6.1	Ref. [70]
$\text{p}K_B$	pK for intracellular buffer	7.5	Based on Ref. [70]
$c_{\text{Na},0}$ (mM)	Na^+ concentration in the medium	145	Physiological condition
$c_{\text{K},0}$ (mM)	K^+ concentration in the medium	9	Physiological condition
$c_{\text{Cl},0}$ (mM)	Cl^- concentration in the medium	105	Physiological condition
$c_{\text{HCO}_3,0}$ (mM)	HCO_3^- concentration in the medium	35	Physiological condition
$c_{\text{G},0}$ (mM)	Glucose concentration in the medium	25	Physiological condition

[a]We employ a value approximately one to two orders of magnitude lower than those documented in water [68,69]. This adjustment considers the crowded cytoplasmic environment full of proteins and organelles and the presence of the nucleus within the confines of a narrow cell. We will demonstrate later that varying D_i by two orders of magnitude does not alter the conclusions drawn in this study (refer to Fig. S4, SM [71]).

back values are adjusted accordingly, i.e., $(\alpha^{\text{f}} + \alpha^{\text{b}})/2 = \alpha$ is fixed.

III. RESULTS AND DISCUSSIONS

A. Brief historical review of the model

This new model builds upon our earlier models. To facilitate insightful discussions and provide adequate context on the new model predictions, we briefly review the historical development of our early models and their key contributions to the scientific field.

Our model started with a two-phase framework, delineating the F-actin and cytosol phases, while incorporating electroneutral solutes that induced osmosis and water flux [27]. This foundational model classified mammalian cell migration into distinct mechanisms: an actin-driven process, propelled by actin polymerization (depolymerization) at the cell leading (trailing) edge, and a water-driven mechanism, powered by water influx (efflux) across the cell membrane. Actin polymerization rate and focal adhesion strength determined the velocity of actin-driven migration, while water flux and the coefficient of extracellular hydraulic resistance influenced water-driven migration [27]. Rigorous analysis revealed that the two-phase model, incorporating solutes, satisfied the energy identity, allowing for a comparative exploration of energy expenditure in actin-driven and water-driven cell migration [28].

To comprehensively capture actin dynamics, G-actin was subsequently integrated into the original two-phase model, resulting in a multi-phase system. This enhancement provided a nuanced perspective on actin dynamics and its interplay with extracellular environments. Our research demonstrated biphasic cell velocity in the strength of focal adhesion [29], a phenomenon observed experimentally but not initially predicted by the two-phase model [27,28]. Additionally, we predicted biphasic cell velocity in the rate of actin depolymerization, linking this observation to the role of myosin in modulating cell motility [30]. Across all models, electroneutral ions were utilized to quantify osmosis and water flux, proving a valid simplification for studying the osmotic impact and successfully predicting cell motility under diverse fluid environments when specific ion species were not a primary concern [16,17].

In parallel, our study of mammalian cell dynamics involved developing models for cell homeostasis and volume regulation, initially centered on sodium, potassium, and chloride ions' impact on cell volume [59]. Subsequent expansions incorporated pH considerations, resulting in a comprehensive mathematical model involving sodium, potassium, chloride, protons, bicarbonate, and buffer solutions [38]—fundamental components of the current work.

The amalgamation of the cell migration model and the cell volume regulation model, encompassing specific ions, pH, and electric potential, emerged from the necessity to elucidate how SELL1 and NHE1 control confined water-driven cell migration [15]. However, the model's predictions were focused on SWLL1 and NHE1, leaving untapped potential unexplored. Thus, the first part of this work is to unveil previously unreported results derived from this highly synthesized model.

Furthermore, recent experimental observations underscore the imperative to integrate biochemical processes (e.g., pH and ion carriers) with mechanical ones (e.g., actin and fluid dynamics) when studying mammalian cell migration. This work introduces these novel couplings, as illustrated by the red arrows in Fig. 1(c) and Eqs. (42) and (43). The second part of this work is dedicated to predicting and uncovering intriguing phenomena resulting from these couplings.

Collectively, this work represents an innovative scientific exploration into the biophysical processes that unite physics, mechanics, biology, and chemistry, shedding light on the underlying mechanisms of confined mammalian cell migration.

B. Primer: A cell without ion carrier polarization

During cell migration driven by actin polymerization, the role of ion dynamics and osmosis becomes noncritical. In such instances, cells migrate even without ion carrier polarization. Within our modeling framework, this scenario is represented by setting the ion carrier permeability to be equal at both the front and back, $\alpha^{\mathrm{b}} = \alpha^{\mathrm{f}}$, for all ion carriers (Sec. II H). The driving force in this context is implemented through a nonzero rate of actin polymerization, $J^{\mathrm{f}}_{\mathrm{actin}}$, at the front of the cell [Eqs. (9)]. With this boundary condition, the model predicts a distribution of F-actin polarizing towards the cell front, and the actin retrograde velocity flows towards the cell back [Fig. S1(A) in Supplemental Material (SM) [71]]. This characteristic actin profile aligns with expectations for actin-driven cell migration [27–30].

In contrast, in the absence of (i) ion carrier polarization, (ii) the coupling between mechanical and biochemical processes, and (iii) extracellular environment polarization, the concentrations of all ion species and electric potential remain uniform within the cell [Fig. S1(A) in SM [71]]. Spatial variations in ions and electrical potential become noteworthy only when the cell or its environment is polarized or when there is a coupling between mechanical and biochemical processes in the cytoplasm. The forthcoming work will delve into exploring these intriguing scenarios.

C. Polarization of ion carriers leads to intracellular gradients

Elongated cells have polarized distributions of ion carriers which enhance cell motility [15,16]. This polarization also induces intracellular pH, electric potential, and osmotic gradients, which we can predict with our model. To begin with, we will remove the coupling between mechanics and chemistry; this coupling will be added later to examine the altered dynamics.

Frontal polarization of NHE plays critical roles in confined migration of human breast cancer and murine sarcoma cancer cells [14–16]. We use NHE as the first example to illustrate how ion carrier polarization leads to intracellular gradients. We vary the NHE polarization ratio from $\alpha^{\mathrm{f}}_{\mathrm{NHE}}/\alpha^{\mathrm{b}}_{\mathrm{NHE}} = 1$, meaning nonpolarized, to $\alpha^{\mathrm{f}}_{\mathrm{NHE}}/\alpha^{\mathrm{b}}_{\mathrm{NHE}} = 3$, meaning a three-folds polarization to the cell front. In human breast cancer cells, 2.3 folds of front NHE polarization was observed [15].

Our model predicts that as the frontal polarization ratio of NHE increases, the intracellular ion gradients increase [Fig. 2(a)]. Higher pH is developed at the cell front than the cell back because NHE continuously removes hydrogen ions at the front. High pH leads to high bicarbonate concentration due to the bicarbonate-carbonic acid pair reaction. As a result, the spatial distributions of pH and bicarbonate concentration mirror each other. In addition, the frontal polarization of NHE brings in sodium at the cell front. Since NHE is electroneutral, based on this modeling framework, its polarization does not generate a significant intracellular electric potential gradient. The predicted trace amount of the intracellular electric potential gradient is due to the coupling between proton and sodium dynamics via NHE. The model predicts that within a physiologically relevant regime, the pH-electric potential interaction is of second-order importance. Nor does it generate an intracellular cytosol pressure gradient or significantly modify the F-actin velocity and concentration [Fig. S1(A) in SM [71]].

The combined gradients of all ion species generate an elevated osmolarity at the cell front [Fig. 2(a)], which drives water influx at the cell front [Fig. 2(b)]. With contributions from water-driven cell migration, the cell velocity increases with NHE polarization as the water flux increases. This NHE-driven water influx is consistent with our understanding that high NHE expression level leads to cell swelling and water flow [21,38,72]. This water flux is predicted to drive G-actin towards the back of the cell, leading to a higher G-actin concentration at the cell back than the front [Fig. 2(a)]. In summary, on the side where the NHE expression level is high, the overall osmolarity is also high but is less acidic. Water flows from the high NHE side to the low side.

Not all ion carriers are equally effective in generating intracellular ion gradients. Our model predicts that the polarization of NHE, AE2, or the passive chloride channel can modulate the pH gradient, but not other ion carriers [Fig. 2(c), ΔpH]. NHE and AE2 involve hydrogen and bicarbonate ions, respectively, and thus directly impact pH. The passive chloride channel affects chloride concentration, which interacts with AE2, thus indirectly affecting pH. Frontal polarization of NHE increases the pH value at the front, whereas AE2 and the passive potassium channel decrease it [Fig. 2(c), pH^{f}]. However, due to their electroneutrality, NHE and AE2 are inefficient in modulating the intracellular electric potential [Fig. 2(c), ϕ^{f} and $\Delta\phi$]. In contrast, the polarization of the passive potassium and chloride channels can affect the electric field significantly because of their high flux and electrogenic nature.

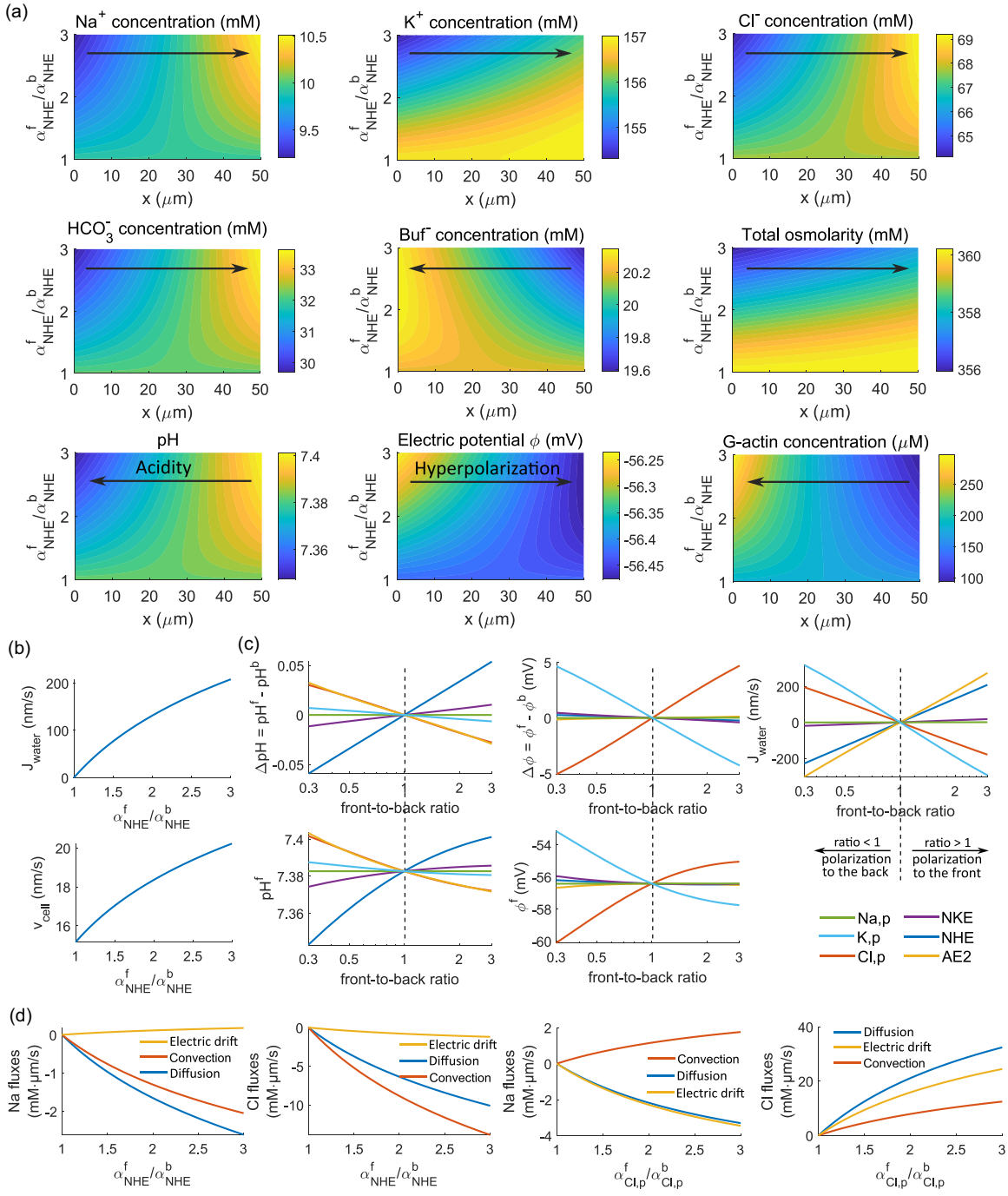

FIG. 2. Model predictions on the effect of polarized ion carriers without coupling between mechanics and biochemistry. (a) Spatial distribution along the cell length (x) of intracellular variables for different degrees of frontal polarization of NHE ($\alpha^{f}_{NHE}/\alpha^{b}_{NHE}$). The arrows indicate the direction of polarization of the fields under the frontal polarization of NHE. (b) Water flux (J_{water}) and cell velocity (v_{cell}) as functions of NHE polarization ($\alpha^{f}_{NHE}/\alpha^{b}_{NHE}$). (c) Intracellular pH difference (ΔpH between the front and back intracellular pH), pH at the cell front (pH^{f}), electric potential difference ($\Delta\phi$ between the front and back intracellular electric potential), electric potential at the cell front (ϕ^{f}), and water flux as functions of the polarization ratio of each ion carrier. A ratio equal to 1 means the ion carriers are not polarized. Each ion carrier is varied independently, while the other carriers remain nonpolarized. (d) The relative contributions from diffusion, convection, and electric drift to the total intracellular fluxes as functions of ion carrier polarization.

The gradient of the intracellular electric field determines the electric drift of each ion species. For ion carriers that do not generate a significant electric potential gradient, such as NHE, their polarization does not lead to the same order of magnitude of electric drift of ions compared to the diffusive and convective fluxes [Fig. 2(d), left two panels]. On the other hand, for ion carriers that are effective in creating an intracellular electric field, such as the passive chloride channel, their

polarization leads to comparable contributions of diffusion, convection, and electric drift [Fig. 2(d), right two panels]. Due to the distinct concentration amplitudes and gradients of different ion species [Fig. 2(a)], the relative contribution of each flux mechanism is also predicted to be different for each species (Fig. 2(d), the other ions are shown in Fig. S2 SM [71]). The model predicts that all three flux mechanisms are equally significant as long as the electric potential gradient is non-negligible. This comparison suggests that the Péclet number is on the order of 1, and the coupling among different biophysical components is effectively working together to generate the cellular response.

Our model predicts that ion carriers that are effective in generating pH or electric potential gradients are also effective in generating water flux [Fig. 2(c), J_{water}]. Frontal polarization of NHE and AE2 leads to water influx at the front (and thus efflux at the back). In contrast, the frontal polarization of the passive potassium and chloride channels leads to water efflux at the front (and thus influx at the back). This model prediction is consistent with experimental observations: frontal polarization of NHE1 and back polarization of SWELL1, a type of passive chloride channel, collectively drive cell migration [15]. AE2 and the passive chloride channel generate intracellular pH gradients along their direction of polarization but create water flux in the opposite direction.

The polarization of NKE, one of the essential ion carriers in maintaining physiological functions, seems to have little effect on intracellular pH and electric potential compared to other ion carriers [Fig. 2(c)]. This does not mean that NKE does not matter. The model predicts that NKE polarization ratio needs to be significantly larger to see differences in the pH gradient, electric potential, and water flux [Fig. S1(B) SM [71]]. When NKE is highly polarized to the back, water flows out of the cell at the back. This directional water flux has also been demonstrated in experiments where kidney cells pump water from the apical to the basal side [11].

D. Extracellular pH polarization leads to intracellular pH gradient via AE2

Extracellular pH gradients can occur *in vivo* in multiple scenarios, such as from solute gradients generated by neighboring cells, fluid circulation in organs, the tumor microenvironment, or during immune response [73]. At the same time, cells migrating in this environment may have polarized ion carriers. We investigate how extracellular pH gradients interact with polarized ion carriers during migration. In the model, we increase the extracellular pH at the front of the cell, pH_0^{f}, while keeping the pH at the back, pH_0^{b}, fixed at 7.42. The increase of pH_0^{f} is obtained by increasing the extracellular bicarbonate concentration at the front.

In cells without ion carrier polarization, the intracellular pH gradient follows the extracellular one [Fig. 3(a)]. This is because increased extracellular bicarbonate concentration at the front leads to less bicarbonate efflux through AE2, and thus increases intracellular bicarbonate concentration at the cell front [Fig. 3(a)]. For this reason, we hypothesize that AE2 is the first responder to the extracellular pH change, and other ion carriers follow the AE2 change instead of following the extracellular cues. We will test this hypothesis later.

Cells have abilities to cushion environmental stress, so the intracellular pH gradient is much smaller than the extracellular one, as predicted by the model. The pH gradient has little effect on the intracellular electric potential [Fig. S3(A) SM [71]]. To show that these model predictions are robust, we artificially place cells into a different state by increasing the permeability of the passive sodium channel, $\alpha_{\text{Na},p}$, by four orders of magnitudes at both front and back. Such a sodium permeability increases intracellular sodium concentration by about 20 mM, creates a positive membrane potential, and alkalizes the intracellular environment [Fig. S3(B) SM [71]]. Despite these nontrivial changes in cell homeostasis, the model predictions remain unchanged: the intracellular pH gradient is smaller than the extracellular one, and the pH gradient has a nonsignificant effect on the intracellular electric potential. The predicted smaller intracellular pH gradient than the extracellular one does not result from the ion diffusivities. Two orders of magnitude increase or decrease of the diffusion coefficient of ions do not increase the predicted intracellular pH gradient, even if the intracellular ion fluxes change [Fig. S4 SM [71]]. This is because the cell responds to the extracellular pH via AE2, not via one-to-one correspondence of pH values. The resultant bicarbonate concentration, the chemical reactions, and the coupling among different components work together to help maintain cell homeostasis.

The spatial gradient of the bicarbonate concentration mirrors that of pH [Fig. 3(a)], as we have seen in the last section [Fig. 2(a)]. Although a frontal polarization of NHE and an extracellular pH increase at the front generate same intracellular pH and bicarbonate gradients, the other ion concentration fields are different between these two scenarios [Figs. 3(a) and 2(a)]. In addition, with increased extracellular pH at the cell front, the model predicts water efflux at the front [Fig. 3(b)], as opposed to influx with NHE polarization [Fig. 2(b)]. These phenomena suggest that the intracellular pH gradient alone does not determine the distribution of ions and the direction of water flux.

We thus expect that the combination of extracellular pH and NHE polarizations generate interesting patterns. Indeed, the model predicts that increasing extracellular pH at the cell front while polarizing NHE towards the back cancels the intracellular pH gradient, but polarizing NHE towards the cell front enhances the positive intracellular pH gradient brought by the high front extracellular pH [Fig. 3(c)]. The water flux follows an opposite pattern such that a frontal polarization of NHE cancels the water flux generated by front extracellular pH increase.

Likewise, the combination of an extracellular pH gradient with the polarization of the passive chloride channel [Fig. 3(d)] or AE2 [Fig. 3(e)] has different effects on generating intracellular pH gradient and water flux. Cells in general can have multiple ion carriers polarized at the same time. Since ion fluxes are additive, the effects from these polarizations are also additive. For example, a frontal polarization of NHE and a back polarization of the passive chloride channels mutually increase water influx at the cell front, whereas frontal polarization of both NHE and the passive chloride channels results in no water flux or even water efflux at the cell front [15].

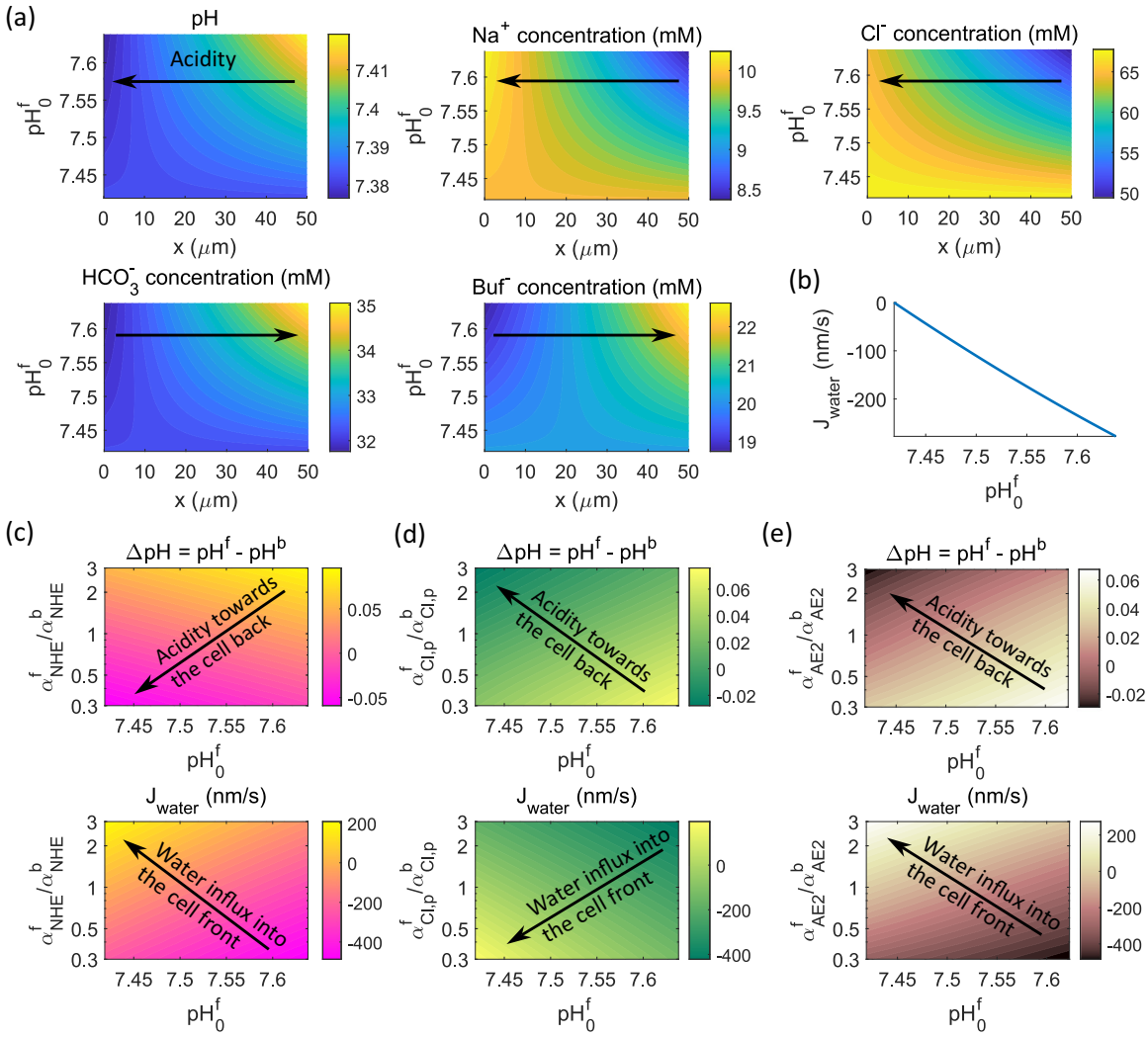

FIG. 3. Model prediction where there is an extracellular pH increase (more alkaline) at the cell front while the pH at the back is fixed. Extracellular pH change is obtained by changing the concentration of extracellular bicarbonate from 35 to 58 mM at the front. Before polarization, $\mathrm{pH}_0^{\mathrm{f}} = \mathrm{pH}_0^{\mathrm{b}} = 7.42$. After polarization, $\mathrm{pH}_0^{\mathrm{f}} > 7.42$ and the value varies. No coupling between mechanics and chemistry. (a) Spatial distribution (x) of intracellular pH and ion concentrations as functions of extracellular pH at the cell front. The arrows indicate the directions of polarization of the fields under the variation of $\mathrm{pH}_0^{\mathrm{f}}$. (b) Water flux at the cell front as a function of extracellular pH at the cell front. [(c)–(e)] The intracellular pH difference (defined as the pH at the cell front minus the back) and water flux at the cell front as functions of ion carrier polarization [NHE in (c)], passive chloride channel in (d), and AE2 in (e) and extracellular pH at the cell front. In (c)–(e), the arrows show the directions of the indicated trends on a two-dimensional parameter space. Under the conservation of mass, water influx into the cell front corresponds to water efflux at the cell back. The cell front is at $x = L$ where actin polymerization happens, and the cell back is at $x = 0$.

To test our hypothesis that AE2 is *the* carrier that responds to the extracellular pH change, we vary the AE2 permeability at the cell front while keeping it unchanged at the back and observe the cell responses in the absence of extracellular pH polarization. The model indeed predicts that a decrease of AE2 permeability at the cell front produces the same intracellular gradients of all field variables as the case of increasing the extracellular pH at the cell front (compare Fig. S5 with Fig. S3 SM [71]). No other ion carriers are able to achieve this. Therefore, from the cell homeostasis regulation perspective, a higher extracellular pH at the cell front (without regulating AE2 activities) is equivalent to reducing AE2 activity at the cell front (without polarizing the extracellular pH).

E. Extracellular electrical potential gradients leads to intracellular gradients via passive potassium channels

We next study the effect of extracellular electric potential gradients by increasing the front potential, ϕ_0^{f}, from 0 to 30 mV while keeping $\phi_0^{\mathrm{b}} = 0$ at the back. In cells without ion carrier polarization, the intracellular electric potential gradient is predicted to follow the extracellular one [Fig. 4(a)] but its gradient is smaller. The electric potential gradient has little effect on pH [Fig. S6(A) SM [71]]. Like the previous case, these results are independent of parameters: Four orders of magnitude increase in the permeability of the passive sodium channel, $\alpha_{\mathrm{Na},p}$, increases the intracellular pH and reverses the polarity of the electric potential, but the impact of the

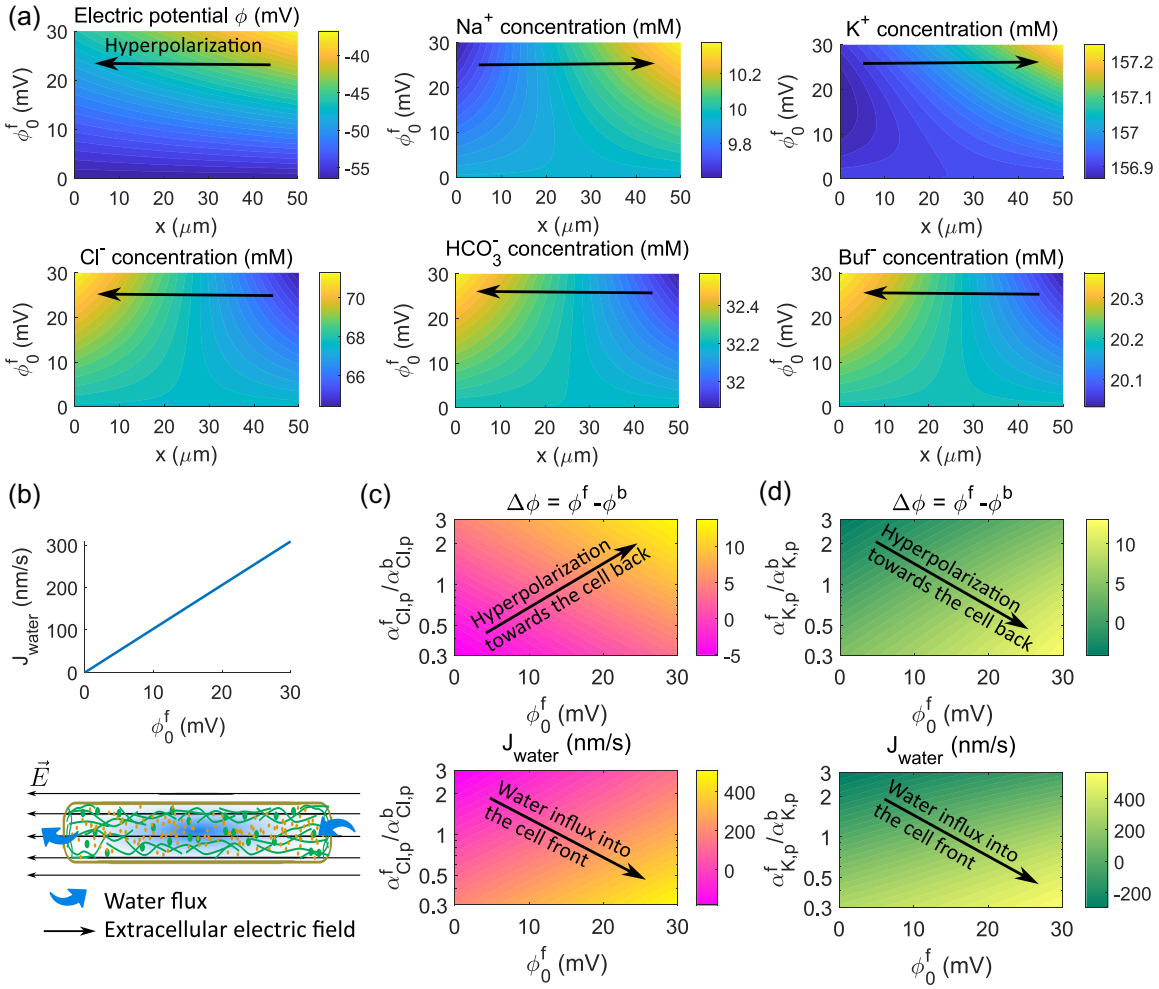

FIG. 4. Model predictions on the effect of extracellular electric potential increase at the cell front while the potential at the back is fixed. Before polarization, $\phi_0^f = \phi_0^b = 0$. After polarization, $\phi_0^f > 0$ and the value varies. No coupling between mechanics and chemistry. (a) Spatial distribution (x) of intracellular electric potential and some ion concentrations as functions of extracellular electric potential at the cell front. The arrows indicate the directions of polarization of the fields under the variation of ϕ_0^f. (b) Water flux into the cell front as the extracellular electric potential increases at the cell front. [(c) and (d)] The intracellular electric potential difference (defined as the potential at the cell front minus the back) and water flux at the cell front as functions of ion carrier polarization [passive chloride channel in (c) and passive potassium channel in (d)] and extracellular electric potential at the cell front. In (c) and (d), the arrows show the directions of the indicated trends on a two-dimensional parameter space. Under the conservation of mass, water influx into the cell front corresponds to water efflux at the cell back. The cell front is at $x = L$ where actin polymerization happens, and the cell back is at $x = 0$.

extracellular electric potential gradient on the intracellular pH remains negligible, and the intracellular electric potential gradient is less than the extracellular one [Fig. S6(B) SM [71]].

A positive extracellular electric potential at the front leads to reduced potassium efflux from the passive potassium channel, generating a relatively high intracellular potassium concentration at the cell front [Fig. 4(a)]. Fluxes through other ion carriers adjust as well, creating intracellular gradients for all ions. However, the gradients of ion concentrations from external electric potential gradients are smaller than those from the pH gradient [compare Figs. 4(a) and 3(a)], although the magnitude of water fluxes from the two cases are comparable [Figs. 4(b) and 3(b)].

The passive chloride and potassium channels are the only two ion carriers whose polarization is able to generate intracellular nontrivial electric potential gradient [Fig. 2(c)]. When these two channels are polarized in the presence of an extracellular electric potential gradient, various patterns of potential gradients and water flux occur [Figs. 4(c) and 4(d)]. For example, a frontal polarization of the chloride channel increases the intracellular electric potential generated by the extracellular potential but reduces or even reverses the water flux. Our model suggests that cells *in vivo* may develop ion carrier polarization to enhance or counter-act environmental electrical signals.

Since passive chloride channels generate an intracellular pH gradient [Fig. 2(c)], but there is almost no intracellular pH gradient under extracellular electric potential polarization [Fig. S6 SM [71]], we thus hypothesize that the passive potassium channel is the agent that responds to the extracellular electric potential signal. We test this hypothesis by varying the permeability of the passive potassium channel at the cell front in the absence of extracellular electric potential polarization. The model predicts that reducing front potassium channel

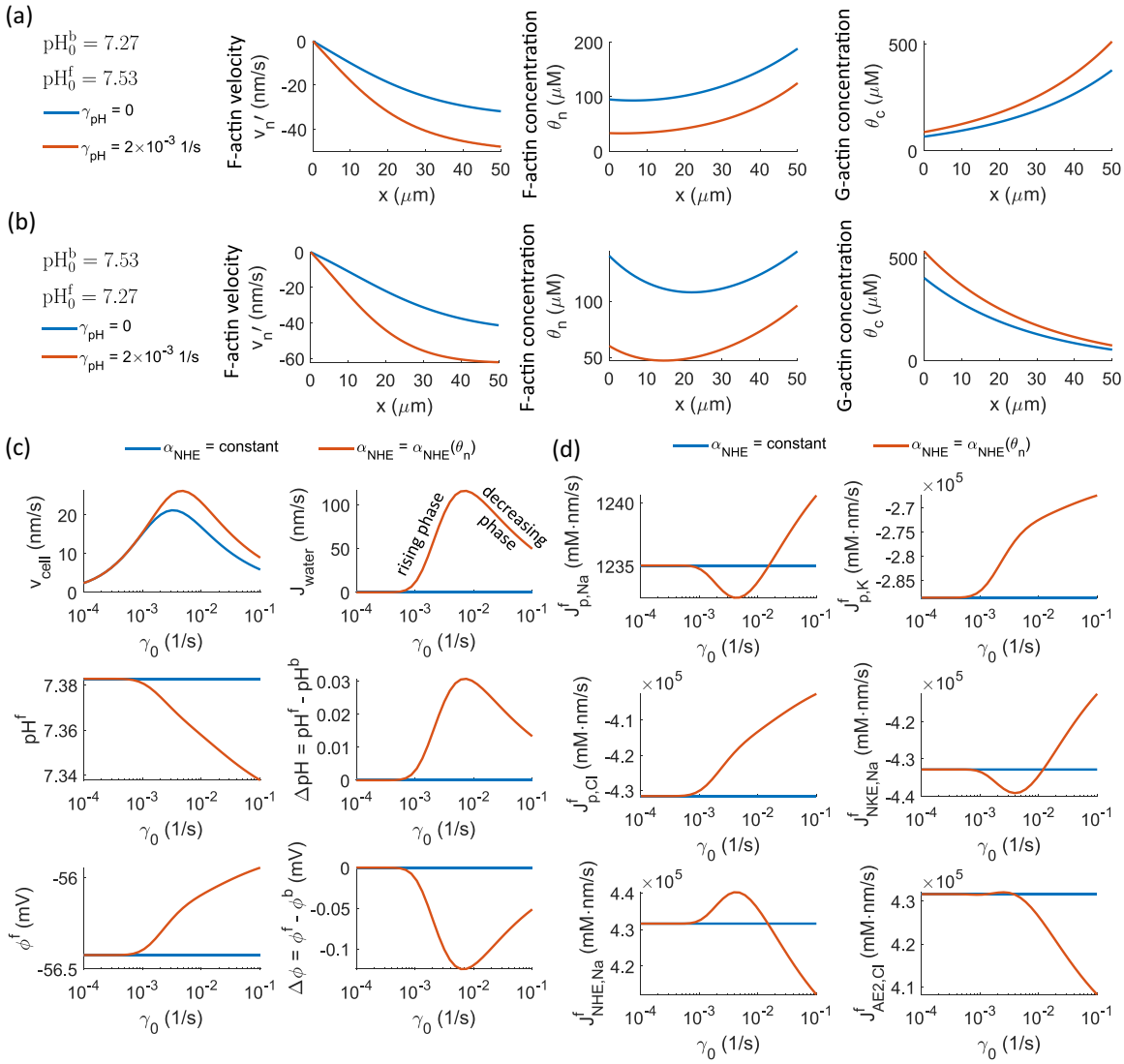

FIG. 5. Effects of coupling among actin depolymerization, pH, and NHE activities. (a) Actin distribution in a polarized extracellular pH environment: $pH_0^f = 7.53$, $pH_0^b = 7.27$, $J^f_{water} = -363$ nm/s from model calculation; and (b) $pH_0^f = 7.27$, $pH_0^b = 7.53$, $J^f_{water} = 363$ nm/s from model calculations. (c) Cell velocity and homeostasis in a nonpolarized environment as functions of a constant rate of actin depolymerization for different NHE permeability choices. (d) Fluxes through ion carriers in a nonpolarized environment as functions of a constant rate of actin depolymerization for different choices of NHE permeability.

activities is equivalent to increasing the extracellular front electric potential (compare Fig. S7 with Fig. S6 SM [71]). All spatial fields have the same directions of gradients, and the water fluxes follow the same direction under these two cases. No other ion carriers can achieve this correspondence.

F. pH-triggered actin depolymerization can modulate F-actin distribution

In the above discussion, we used a decoupled model between actin and pH [$\gamma = \gamma_0 =$ const. and $\gamma_{pH} = 0$ in Eq. (42)] to analyze how each ion carrier impacts cell homeostasis. In this section, we will study the effect of pH-dependent actin depolymerization on the F-actin distribution. Recall that polarization of extracellular pH leads to membrane water flux [Fig. 3(b)]. Water flux generates cytosol flow, which impacts actin distribution in two ways.

The first effect comes from the convection of G-actin by the cytosol flow. When the cytosol flows from the back to the front of the cell, which happens when $pH_0^f > pH_0^b$, it carries G-actin and polarizes it towards the front [Fig. 5(a)]. When the opposite occurs, G-actin polarizes to the back [Fig. 5(b)]. The second effect is on F-actin concentration influenced by G-actin. In the simplest case with no environment or ion carrier polarization, F-actin always concentrates at the cell front where actin polymerization occurs [Fig. S1(A) SM [71]]. This frontal F-actin polarization can be critical in actin-driven cell migration [29,30,74]. However, when G-actin polarizes towards the back, which occurs when cytosol flows from the front to the back, F-actin can redistribute [Fig. 5(b)].

The F-actin distribution can revert when the rate of actin depolymerization γ increases with pH by cofilin [58,75]. Since the intracellular pH gradient follows the extracellular one, so does the actin depolymerization rate. When

$pH_0^f > pH_0^b$, a higher rate of actin depolymerization at the cell front does not change the polarity of F-actin [Fig. 5(a)]. When $pH_0^f < pH_0^b$, the higher rate of actin depolymerization at the cell back disassembles F-actin, leading to a frontal polarization of the cell [Fig. 5(b)] similar to that in the control case [Fig. S1 SM [71]].

The model suggests that pH can modulate F-actin distribution through pH-induced cytosol flow, pH-dependent actin depolymerizatoin, or both. Since actin distribution is critical to cell motility, modulating intracellular dynamics, and force distribution, the coupling between pH and actin can be one of the mechanisms to ensure proper cell function when there is environmental pH shocks.

G. Actin-generated NHE polarization generates biphasic water flux and intracellular pH gradient

We have so far prescribed ion carriers' polarization by setting their front-to-back polarization ratios as parameters. In this section, we consider the case where NHE polarization is determined by F-actin [16,21], i.e., $\alpha_{NHE} = \alpha_{NHE}(\theta_n)$ [Eq. (43)], instead of being prescribed. In order to focus on the effect of actin-induced NHE polarization, we let $\gamma = \gamma_0 = \text{const.}$, and the other ion carriers and the extracellular environment are nonpolarized.

Without actin-induced NHE polarization, there is no water flux nor intracellular ion gradients regardless of the rate of actin depolymerization, γ, in a nonpolarized cell [Figs. 5(c) and 5(d)]. The cell velocity is a biphasic function of γ because of an actin-flow to actin-distribution transition [30]. The rate of actin depolymerization, γ, reduces the average F-actin concentration across the cell and establishes a high F-actin polarization ratio, i.e., θ_n^f/θ_n^b increases with γ [30]. After implementing actin-induced NHE polarization where the permeabilities α_{NHE}^f and α_{NHE}^b follow θ_n^f and θ_n^b, NHE polarizes towards the cell front as the rate of actin depolymerization, γ, increases. The model predicts a biphasic water flux as a function of actin depolymerization rate, γ [Fig. 5(c)]. The rising phase in the water flux comes from the increasing ratio of NHE polarization as γ increases. The decreasing phase is due to reduced NHE flux as F-actin concentration drops. In this case, even if the NHE polarization ratio is very large, the low NHE flux cannot establish a large osmotic gradient. Biphasic water flux contributes to biphasic cell velocity [Fig. 5(c)].

The three ion carriers that involve sodium ions, NHE, NKE, and the passive sodium channel, also show biphasic fluxes as γ increases. Ion carriers that do not involve sodium are monotonic in γ, except for AE2, where a small bump appears due to its linkage to pH [Fig. 5(d)]. With the actin-NHE coupling, our model indicates that F-actin alone can generate water flux and ion dynamics without prescribing polarization for other membrane ion carriers. This result is surprising and suggest that the actin-NHE interaction is the central element in establishing cell movement. The gradients of intracellular pH and electric potential also show biphasic relations with the rate of actin depolymerization [Fig. 5(c), ΔpH and $\Delta\phi$] but not the baseline pH and electric potential values [Fig. 5(c), pH^f and ϕ^f]. This difference suggests that pH and electric potential gradients are influenced by both the NHE polarization ratio and absolute permeability. In contrast, pH and electric potential values are only affected by NHE absolute flux. The decreasing pH with increasing γ indicates that cells will not further elevate actin depolymerization through pH-γ coupling.

IV. CONCLUSIONS

In this work, we used a theoretical model to study the impact of ion carriers and extracellular environment gradients on cell ion homeostasis, migration, and actin network distribution. Each ion carrier plays a specific role in maintaining cell homeostasis by communicating information between the inside and the outside. Some ion carriers modulate pH, some modulate electric potential, and some do both. The model predicts that pH and electric potential are uncoupled on the first order, suggesting that cells can maintain homeostasis of one field to a satisfactory extent when the other field is perturbed. The coupling of the system can generate a second-order impact between pH and electric potential. Based on this model prediction of the physiologically relevant range of cell homeostasis, the second-order impact is insignificant. It is possible that a model with additional bio-chemo-physical processes can predict a stronger coupling between pH and electric potential.

Our results show that, within the ion carriers included in this work, extracellular pH gradients lead to intracellular pH gradient via chloride-bicarbonate exchangers, whereas extracellular electric potential polarization leads to intracellular electric potential gradient via passive potassium channels. The magnitudes of intracellular gradients are smaller than the extracellular ones, indicating that cells can cushion environmental changes through negative feedback.

Cells develop intracellular pH, electric potential, and ion concentration gradients when membrane ion carriers are polarized. The magnitudes of these gradients depend on the ratio of carrier polarization. The types of membrane ion carriers also play a major role in determining the gradients. Given the same polarization ratio, NHE, AE2, and the passive chloride and potassium channels are more effective in creating intracellular biochemical gradients than NKE and the passive sodium channel. When ion carrier polarization is coupled with extracellular polarization, various combinations of intracellular electric potential gradient, pH gradient, and water flux can occur. It is possible to create an intracellular gradient without generating water flux, or generate water flux without creating an intracellular gradient. When extracellular hydraulic resistance is high, water flux will increase the cell migrations speed.

The coupling between the actin network and ion carriers introduces more complexity and increases the diversity of behaviors we observe. Our model predicts that the polarization of F-actin concentration can change when an intracellular pH gradient develops. The distribution of F-actin is related to many intracellular processes, such as force distribution, morphology, nucleus anchoring, nuclear envelope stress, and intracellular trafficking. In addition to the known impact of pH on cell biochemistry, the model suggests that pH also has the potential to indirectly affect cell dynamics through a redistribution of the actin network.

The structural linkage between F-actin and NHE through ezrin suggests that the polarization of F-actin establishes NHE polarization. The polarization of F-actin comes from actin polymerization, and the polarization of NHE leads to water flux. As a result, actin-driven cell migration and water-driven cell migration are intrinsically coupled together. In two-dimensional cell migration, where water-driven cell migration is not applicable due to the low extracellular hydraulic resistance, we can still expect intracellular cytosol flow generated by transmembrane water flux. Such cytosol flow has the potential to provide effective convection for intracellular signaling molecules. Moreover, our model predicts that F-actin alone can generate water flux through NHE, even when other membrane ion carriers are not polarized. This result is surprising and suggest that the actin-NHE interaction is the central element in establishing cell movement.

In several of our model predictions, we distinguish between average concentration and gradient, as these two parameters carry distinct biophysical significance in cellular dynamics. The total or average concentration of F-actin, for instance, influences the magnitude of the force from focal adhesion to the cell body. In contrast, the F-actin gradient signifies the degree of F-actin polarization within the cell, establishing connections with the polarization of other biophysical processes. Concerning ions, the total or average concentrations impact biophysical processes reliant on the absolute quantity of ions. For instance, the intracellular proton concentration determines the pH within the cell, a critical factor for cellular function. In contrast, concentration gradients of ions contribute to the establishment of cell polarization and osmolarity gradients, subsequently influencing water flux across the cell. Our model predictions highlight that in the presence of ion carrier polarization, variations between average and gradient concentrations can occur. This underscores the intricate and multifaceted role played by ion carriers in cellular processes.

To summarize, based on our model predictions, membrane ion carriers and environmental polarizations can generate intracellular osmotic, electric potential, pH, and actin gradients, which have implications for intracellular dynamics and signaling. The coupling between biochemistry and mechanics further enhances the cells' adaptability to internal or external perturbations. The future development of understanding cell biology requires integrated views of biochemical and physical processes.

ACKNOWLEDGMENTS

Yizeng Li is supported by NSF 2303648. Sean X. Sun is supported by NIH R01GM134542. The opinions, findings, and conclusions, or recommendations expressed are those of the authors and do not necessarily reflect the views of any of the funding agencies.

[1] P. Friedl and D. Gilmour, Collective cell migration in morphogenesis, regeneration and cancer, Nat. Rev. Mol. Cell Biol. **10**, 445 (2009).

[2] A. Riga, V. G. Castiglioni, and M. Boxem, New insights into apical-basal polarization in epithelia, Curr. Opin. Cell Biol. **62**, 1 (2020).

[3] K. M. Yamada, A. D. Doyle, and J. Lu, Cell–3D matrix interactions: Recent advances and opportunities, Trends Cell Biol. **32**, 883 (2022).

[4] Y. Mori, A. Jilkine, and L. Edelstein-Keshet, Wave-pinning and cell polarity from a bistable reaction-diffusion system, Biophys. J. **94**, 3684 (2008).

[5] H. Wang, Y. Li, J. Yang, X. Duan, P. Kalab, S. X. Sun, and R. Li, Symmetry breaking in hydrodynamic forces drives meiotic spindle rotation in mammalian oocytes, Sci. Adv. **6**, eaaz5004 (2020).

[6] C. Copos and A. Mogilner, A hybrid stochastic-deterministic mechanochemical model of cell polarization, Mol. Biol. Cell **31**, 1637 (2020).

[7] S. P. Banavar, M. Trogdon, B. Drawert, T.-M. Yi, L. R. Petzold, and O. Campàs, Coordinating cell polarization and morphogenesis through mechanical feedback, PLoS Comput. Biol. **17**, e1007971 (2021).

[8] F. Tostevin, M. Wigbers, L. Søgaard-Andersen, and U. Gerland, Four different mechanisms for switching cell polarity, PLoS Comput. Biol. **17**, e1008587 (2021).

[9] S. SenGupta, C. A. Parent, and J. E. Bear, The principles of directed cell migration, Nat. Rev. Mol. Cell Biol. **22**, 529 (2021).

[10] R. Zhao, A. Afthinos, T. Zhu, P. Mistriotis, Y. Li, S. A. Serra, Y. Zhang, C. L. Yankaskas, S. He, M. A. Valverde, S. X. Sun, and K. Konstantopoulos, Cell sensing and decision-making in confinement: The role of TRPM7 in a tug of war between hydraulic pressure and cross-sectional area, Sci. Adv. **5**, eaaw7243 (2019).

[11] M. I. Choudhury, Y. Li, P. Mistriotis, A. C. N. Vasconcelos, E. E. Dixon, J. Yang, M. Benson, D. Maity, R. Walker, L. Martin, F. Koroma, F. Qian, K. Konstantopoulos, O. M. Woodward, and S. X. Sun, Kidney epithelial cells are active mechano-biological fluid pumps, Nat. Commun. **13**, 2317 (2022).

[12] Y. Li, K. Konstantopoulos, R. Zhao, Y. Mori, and S. X. Sun, The importance of water and hydraulic pressure in cell dynamics, J. Cell Sci. **133**, jcs240341 (2020).

[13] Y. Li and S. X. Sun, Fundamental mechanics of cell shape and cell movement, in *Cell Movement in Health and Disease* (Elsevier, London, 2022), pp. 85–100.

[14] K. M. Stroka, H. Jiang, S.-H. Chen, Z. Tong, D. Wirtz, S. X. Sun, and K. Konstantopoulos, Water permeation drives tumor cell migration in confined microenvironments, Cell **157**, 611 (2014).

[15] Y. Zhang, Y. Li, K. N. Thompson, K. Stoletov, Q. Yuan, K. Bera, S. J. Lee, R. Zhao, A. Kiepas, Y. Wang, P. Mistriotis, S. A. Serra, J. D. Lewis, M. A. Valverde, S. S. Martin, S. X. Sun, and K. Konstantopoulos, Polarized NHE1 and SWELL1 regulate migration direction, efficiency and metastasis, Nat. Commun. **13**, 6128 (2022).

[16] K. Bera, A. Kiepas, I. Godet, Y. Li, P. Mehta, B. Ifemembi, C. D. Paul, A. Sen, S. A. Serra, K. Stoletov, J. Tao, G. Shatkin, S. J. Lee, Y. Zhang, A. Boen, P. Mistriotis, D. M. Gilkes, J. D. Lewis, C.-M. Fan, A. P. Feinberg *et al.*, Extracellular fluid

viscosity enhances cell migration and cancer dissemination, Nature (London) **611**, 365 (2022).
[17] D. Maity, K. Bera, Y. Li, Z. Ge, Q. Ni, K. Konstantopoulos, and S. X. Sun, Extracellular hydraulic resistance enhances cell migration, Adv. Sci. **9**, 2200927 (2022).
[18] B. A. Webb, M. Chimenti, M. P. Jacobson, and D. L. Barber, Dysregulated ph: A perfect storm for cancer progression, Nat. Rev. Cancer **11**, 671 (2011).
[19] M. Ritter, P. Schratzberger, H. Rossmann, E. Wöll, K. Seiler, U. Seidler, N. Reinisch, C. M. Kähler, H. Zwierzina, H. J. Lang, F. Lang, M. Paulmichl, and C. J. Wiedermann, Effect of inhibitors of Na^+/H^+-exchange and gastric H^+/K^+ ATPase on cell volume, intracellular ph and migration of human polymorphonuclear leucocytes, Br. J. Pharmacol. **124**, 627 (1998).
[20] S. Saha, T. L. Nagy, and O. D. Weiner, Joining forces: Crosstalk between biochemical signalling and physical forces orchestrates cellular polarity and dynamics, Philos. Trans. R. Soc. B **373**, 20170145 (2018).
[21] P. G. Vallés, V. Bocanegra, A. G. Lorenzo, and V. V. Costantino, Physiological functions and regulation of the Na^+/H^+ exchanger NHE1 in renal tubule epithelial cells, Kidney Blood Press. Res. **40**, 452 (2015).
[22] C. Li, Q. Qiu, M. Liu, X. Liu, L. Hu, X. Luo, C. Lai, D. Zhao, H. Zhang, X. Gao, Y. Deng, and Y. Song, Sialic acid-conjugate modified liposomes targeting neutrophils for improved tumour therapy, Biomater. Sci. **8**, 2189 (2020).
[23] A. Jeyaram, T. N. Lamichhane, S. Wang, L. Zou, E. Dahal, S. M. Kronstadt, D. Levy, B. Parajuli, D. R. Knudsen, W. Chao, and S. M. Jay, Enhanced loading of functional miRNA cargo via pH gradient modification of extracellular vesicles, Molecular Therapy **28**, 975 (2020).
[24] P. Mistriotis, E. O. Wisniewski, K. Bera, J. Keys, Y. Li, S. Tuntithavornwat, R. A. Law, N. A. Perez-Gonzalez, E. Erdogmus, Y. Zhang, R. Zhao, S. X. Sun, P. Kalab, J. Lammerding, and K. Konstantopoulos, Confinement hinders motility by inducing rhoa-mediated nuclear influx, volume expansion, and blebbing, J. Cell Biol. **218**, 4093 (2019).
[25] R. J. Petrie, N. Gavara, R. S. Chadwick, and K. M. Yamada, Nonpolarized signaling reveals two distinct modes of 3D cell migration, J. Cell Biol. **197**, 439 (2012).
[26] R. J. Petrie, H. Koo, and K. M. Yamada, Generation of compartmentalized pressure by a nuclear piston governs cell motility in a 3D matrix, Science **345**, 1062 (2014).
[27] Y. Li and S. X. Sun, Transition from actin-driven to water-driven cell migration depends on external hydraulic resistance, Biophys. J. **114**, 2965 (2018).
[28] Y. Li, L. Yao, Y. Mori, and S. X. Sun, On the energy efficiency of cell migration in diverse physical environments, Proc. Natl. Acad. Sci. USA **116**, 23894 (2019).
[29] L. Yao and Y. Li, Effective force generation during mammalian cell migration under different molecular and physical mechanisms, Front. Cell Dev. Biol. **10**, 903234 (2022).
[30] L. Yao, Y. Mori, S. X. Sun, and Y. Li, On the role of myosin-induced actin depolymerization during cell migration, Mol. Biol. Cell **34**, ar62 (2023).
[31] D. Maity, Y. Li, Y. Chen, and S. X. Sun, Response of collagen matrices under pressure and hydraulic resistance in hydrogels, Soft Matter **15**, 2617 (2019).
[32] J. Stricker, T. Falzone, and M. L. Gardel, Mechanics of the f-actin cytoskeleton, J. Biomech. **43**, 9 (2010).
[33] B. L. Bangasser, G. A. Shamsan, C. E. Chan, K. N. Opoku, E. Tüzel, B. W. Schlichtmann, J. A. Kasim, B. J. Fuller, B. R. McCullough, S. S. Rosenfeld, and D. J. Odde, Shifting the optimal stiffness for cell migration., Nat. Commun. **8**, 15313 (2017).
[34] S. Walcott and S. X. Sun, A mechanical model of actin stress fiber formation and substrate elasticity sensing in adherent cells., Proc. Natl. Acad. Sci. USA **107**, 7757 (2010).
[35] D.-H. Kim and D. Wirtz, Focal adhesion size uniquely predicts cell migration, FASEB J. **27**, 1351 (2013).
[36] E. A. Cavalcanti-Adam, T. Volberg, A. Micoulet, H. Kessler, B. Geiger, and J. P. Spatz, Cell spreading and focal adhesion dynamics are regulated by spacing of integrin ligands., Biophys. J. **92**, 2964 (2007).
[37] E. L. Barnhart, K.-C. Lee, K. Keren, A. Mogilner, and J. A. Theriot, An adhesion-dependent switch between mechanisms that determine motile cell shape, PLoS Biol. **9**, e1001059 (2011).
[38] Y. Li, X. Zhou, and S. X. Sun, Hydrogen, bicarbonate, and their associated exchangers in cell volume regulation, Front. Cell Dev. Biol. **9**, 683686 (2021).
[39] Y. Li, Y. Mori, and S. X. Sun, Flow-driven cell migration under external electric fields, Phys. Rev. Lett. **115**, 268101 (2015).
[40] B. Martinac, Mechanosensitive ion channels: Molecules of mechanotransduction, J. Cell Sci. **117**, 2449 (2004).
[41] D. C. Gadsby, J. Kimura, and A. Noma, Voltage dependence of Na/K pump current in isolated heart cells., Nature (London) **315**, 63 (1985).
[42] J. Gao, R. T. Mathias, I. S. Cohen, and G. J. Baldo, Two functionally different Na/K pumps in cardiac ventricular myocytes., J. Gen. Physiol. **106**, 995 (1995).
[43] A. Bueno-Orovio, C. Sánchez, E. Pueyo, and B. Rodriguez, Na/K pump regulation of cardiac repolarization: Insights from a systems biology approach., Pflugers Arch. **466**, 183 (2014).
[44] P. M. Cala, Volume regulation by amphiuma red blood cells. the membrane potential and its implications regarding the nature of the ion-flux pathways., J. Gen. Physiol. **76**, 683 (1980).
[45] A. C. Ericson and K. R. Spring, Volume regulation by necturus gallbladder: apical Na^+-H^+ and Cl^--HCO_3^- exchange, Am. J. Physiol. Cell Physiol. **243**, C146 (1982).
[46] S. Grinstein, W. Furuya, and E. J. Cragoe Jr, Volume changes in activated human neutrophils: the role of Na^+/H^+ exchange, J. Cell. Physiol. **128**, 33 (1986).
[47] E. Maeno, N. Takahashi, and Y. Okada, Dysfunction of regulatory volume increase is a key component of apoptosis, FEBS Lett. **580**, 6513 (2006).
[48] A. L. H. Hughes, A. Pakhomova, and P. D. Brown, Regulatory volume increase in epithelial cells isolated from the mouse fourth ventricle choroid plexus involves Na^+–H^+ exchange but not Na^+–K^+–$2Cl^-$ cotransport, Brain Res. **1323**, 1 (2010).
[49] R. T. Alexander and S. Grinstein, Na^+/H^+ exchangers and the regulation of volume, Acta Physiol. **187**, 159 (2006).
[50] W. Scholz, U. Albus, L. Counillon, H. Gögelein, H.-J. Lang, W. Linz, A. Weichert, and B. A. Schölkens, Protective effects of HOE642, a selective sodium-hydrogen exchange subtype 1 inhibitor, on cardiac ischaemia and reperfusion, Cardiovasc. Res. **29**, 260 (1995).
[51] G. Lauritzen, C.-M. Stock, J. Lemaire, S. F. Lund, M. F. Jensen, B. Damsgaard, K. S. Petersen, M. Wiwel, L. Rønnov-Jessen, A. Schwab, and S. F. Pedersen, The Na^+/H^+ exchanger NHE1, but

not the Na^+, HCO_3-cotransporter NBCn1, regulates motility of MCF7 breast cancer cells expressing constitutively active ErbB2, Cancer Lett. **317**, 172 (2012).

[52] G. Chang, J. Wang, H. Zhang, Y. Zhang, C. Wang, H. Xu, Y. Lin, L. Ma, Q. Li, and T. Pang, Cd44 targets Na^+/H^+ exchanger 1 to mediate MDA-MB-231 cells' metastasis via the regulation of ERK1/2, Br. J. Cancer **110**, 916 (2014).

[53] R. L. Mahnensmith and P. S. Aronson, The plasma membrane sodium-hydrogen exchanger and its role in physiological and pathophysiological processes., Circ. Res. **56**, 773 (1985).

[54] M. Karmazyn, NHE-1: Still a viable therapeutic target, J. Mol. Cell. Cardiol. **61**, 77 (2013).

[55] J. R. Casey, S. Grinstein, and J. Orlowski, Sensors and regulators of intracellular pH, Nat. Rev. Mol. Cell Biol. **11**, 50 (2010).

[56] V. Pang, L. Counillon, D. Lagadic-Gossmann, M. Poet, J. Lacroix, O. Sergent, R. Khan, and C. Rauch, On the role of the difference in surface tensions involved in the allosteric regulation of NHE-1 induced by low to mild osmotic pressure, membrane tension and lipid asymmetry, Cell Biochem. Biophys. **63**, 47 (2012).

[57] L. Blanchoin, T. D. Pollard, and R. D. Mullins, Interactions of ADF/cofilin, Arp2/3 complex, capping protein and profilin in remodeling of branched actin filament networks, Curr. Biol. **10**, 1273 (2000).

[58] N. Yonezawa, E. Nishida, and H. Sakai, pH control of actin polymerization by cofilin., J. Biol. Chem. **260**, 14410 (1985).

[59] F. Yellin, Y. Li, V. K. A. Sreenivasan, B. Farrell, M. Johny, D. Yue, and S. X. Sun, Electromechanics and volume dynamics in non-excitable tissue cells, Biophys. J. **114**, 2231 (2018).

[60] M. Dembo and F. Harlow, Cell motion, contractile networks, and the physics of interpenetrating reactive flow, Biophys. J. **50**, 109 (1986).

[61] J. L. McGrath, Y. Tardy, C. F. Dewey, Jr., J. J. Meister, and J. H. Hartwig, Simultaneous measurements of actin filament turnover, filament fraction, and monomer diffusion in endothelial cells, Biophys. J. **75**, 2070 (1998).

[62] D. Zicha, I. M. Dobbie, M. R. Holt, J. Monypenny, D. Y. H. Soong, C. Gray, and G. A. Dunn, Rapid actin transport during cell protrusion, Science **300**, 142 (2003).

[63] D. McDonald, G. Carrero, C. Andrin, G. de Vries, and M. J. Hendzel, Nucleoplasmic β-actin exists in a dynamic equilibrium between low-mobility polymeric species and rapidly diffusing populations, J. Cell Biol. **172**, 541 (2006).

[64] T. Kiuchi, T. Nagai, K. Ohashi, and K. Mizuno, Measurements of spatiotemporal changes in g-actin concentration reveal its effect on stimulus-induced actin assembly and lamellipodium extension, J. Cell Biol. **193**, 365 (2011).

[65] R. L. Satcher and C. F. Dewey, Theoretical estimates of mechanical properties of the endothelial cell cytoskeleton, Biophys. J. **71**, 109 (1996).

[66] T. D. Pollard, L. Blanchoin, and R. D. Mullins, Molecular mechanisms controlling actin filament dynamics in nonmuscle cells, Annu. Rev. Biophys. Biomol. Struct. **29**, 545 (2000).

[67] H. Jiang and S. X. Sun, Cellular pressure and volume regulation and implications for cell mechanics, Biophys. J. **105**, 609 (2013).

[68] V. M. M. Lobo, A. C. F. Ribeiro, and L. M. P. Verissimo, Diffusion coefficients in aqueous solutions of potassium chloride at high and low concentrations, J. Mol. Liq. **78**, 139 (1998).

[69] N. Agmon, The grotthuss mechanism, Chem. Phys. Lett. **244**, 456 (1995).

[70] A. M. Weinstein, A mathematical model of the rat proximal tubule, Am. J. Physiol. Renal Physiol. **250**, F860 (1986).

[71] See Supplemental Material at http://link.aps.org/supplemental/10.1103/PhysRevResearch.6.023158 for supplementary figures.

[72] T. L. Nagy, E. Strickland, and O. D. Weiner, Neutrophils actively swell to potentiate rapid migration, bioRxiv (2023), doi:10.1101/2023.05.15.540704.

[73] L. Oster, J. Schröder, M. Rugi, S. Schimmelpfennig, S. Sargin, A. Schwab, and K. Najder, Extracellular pH controls chemotaxis of neutrophil granulocytes by regulating leukotriene B4 production and Cdc42 signaling, J. Immunol. **209**, 136 (2022).

[74] N. Ofer, A. Mogilner, and K. Keren, Actin disassembly clock determines shape and speed of lamellipodial fragments, Proc. Natl. Acad. Sci. USA **108**, 20394 (2011).

[75] H. Wioland, A. Jegou, and G. Romet-Lemonne, Quantitative variations with pH of actin depolymerizing factor/Cofilin's multiple actions on actin filaments, Biochemistry **58**, 40 (2019).